# Stochastic energy optimization of residential heat pumps in uncertain electricity markets

Golmohammadi, Hessam

*Published in:*
Applied Energy

*DOI (link to publication from Publisher):*
10.1016/j.apenergy.2021.117629



*Publication date:*
2021

*Document Version*
Publisher's PDF, also known as Version of record

Applied Energy 303 (2021) 117629

Contents lists available at ScienceDirect

Applied Energy

journal homepage: www.elsevier.com/locate/apenergy

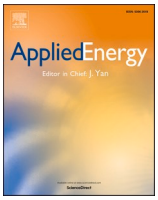

# Stochastic energy optimization of residential heat pumps in uncertain electricity markets

Hessam Golmohamadi

*Department of Computer Science, Aalborg University, 9220 Aalborg, Denmark*

## HIGHLIGHTS

- Flexibility of thermal inertia of buildings with multi-temperature zones.
- Unlocking flexibility potentials of closed-cycle and open-cycle water tanks.
- Characterizing uncertain energy price, ambient temperature, hot water consumption.

## ARTICLE INFO

*Keywords:*
Electricity market
Flexibility
Heat pump
Residential building
Stochastic
Uncertainty

## ABSTRACT

The penetration of renewable energy sources is increasing in power systems all over the world. Due to the intermittency and volatility of renewable energies, demand-side management is a practical solution to overcome the problem. This paper proposes a stochastic model predictive control for heat pumps to supply space heating and domestic hot water consumption of residential buildings. Continuous-Time Stochastic Model is coded in R language to address the model identification approach. The approach uses the sensor data of households to extract the thermal dynamics of the building. The controller participates in three floors of power markets with high renewable power penetration. The three-stage stochastic programming is suggested to unlock power-to-heat flexibility in the day-ahead, intraday, and balancing markets on long, mid, and short advance notices, respectively. Regarding the close correlation between renewable power availability and electricity price, the price data is modeled as probabilistic scenarios through Auto-Regressive Integrated Moving Average. The ambient temperature, as well as the domestic hot water consumption, are addressed as envelope-bounds with upper and lower thresholds. Finally, the operational strategies of the controller are examined on a 150 $m^2$ test house under uncertain electricity prices, weather variables, and occupancy patterns.

In this section, the main nomenclatures are described. However, complementary explanations are described in the text close to the associated mathematical models.

## 1. Introduction

### 1.1. Motivation

In the last years, the share of Renewable Energy Sources (RES) has increased from 125 GW in 2013 to approximately 200 GW in 2020 in power systems worldwide [1]. In this way, the intermittency and volatility of the supply-side increase considerably. To overcome the intermittent renewable energies, demand flexibility is a practical solution. The demand flexibility reflects the part of electricity consumption that can be adjusted (increased/decreased/curtailed/shifted) in response to an external request, e.g. Demand Response (DR). To redress the power system imbalances, all the demand sectors, including residential [2], agricultural [3], industrial [4], and electric vehicles [5], should take part in DR programs. In other words, the segregated demand flexibilities fail to meet the flexibility requirements of the supply side. To provide a general insight into the problem, Fig. 1 depicts a schematic diagram of demand-side flexibility in power systems. In the residential sector, the thermostatically-controlled appliances, e.g. water heaters and heat pumps, have great flexibility potentials [6]. In the agricultural sector, the water irrigation pumps with variable frequency drives offer power flexibility for the power grid [7]. In the industrial sector, the interruptible industrial processes can be turned on/off in response to power excess/shortage in the power market [8]. Regarding the Plug-In Electric Vehicles (PEV), the private and public parking lots are considered virtual power plants to provide power flexibility in the opposite direction of

*E-mail address:* hessamgolmoh@cs.aau.dk.

https://doi.org/10.1016/j.apenergy.2021.117629
Received 23 March 2021; Received in revised form 30 June 2021; Accepted 13 August 2021
Available online 24 August 2021

**Nomenclature**

*Acronyms*

| | |
|---|---|
| ARIMA | Auto-Regressive Integrated Moving Average |
| CCWT | Closed-Cycle Water Tank |
| COP | Coefficient of Performance |
| CTSM | Continuous-Time Stochastic Model |
| DHW | Domestic Hot Water |
| DR | Demand Response |
| EMPC | Economic Model Predictive Control |
| MO | Meteorological Office |
| MPC | Model Predictive Control |
| OCWT | Open-Cycle Water Tank |
| PCM | Phase Change Materials |
| PSO | Power System Operator |
| PEV | Plug-in Electric Vehicle |
| RES | Renewable Energy Source |
| SEMPC | Stochastic Economic Model Predictive Control |

*Indices*

| | |
|---|---|
| n | Index for DHW consumers, $n = 1,\ldots,N$ |
| r | Index for building rooms, $r = 1,\ldots,R$ |
| t | Index for time slots, $t = 1,\ldots,N_\tau$ |
| ω | Index for price scenarios, $\omega = 1,\ldots,N_\omega$ |

*Constants*

| | |
|---|---|
| $\dot{m}_{DHW}^{n}$ | Mass flow of DHW for consumer n (kg/s) |
| $\Pi_S^r$ | Heating power captured by solar irradiation (kW) |
| $\Pi_t^{Rated}$ | Rated power demand of the compressor of the heat pump (kW) |
| $C_h^r$ | Heat capacity of heating system for room r (kWh/°C) |
| $C_e^r$ | Heat capacity of an envelope for room r (kWh/ °C) |
| $C_i^r$ | Heat capacity of indoor temperature for room r (kWh/°C) |
| $C_w^{CC}$ | Heat capacity of CCWT (kWh/°C) |
| $C_w^{OC}$ | Heat capacity of OCWT (kWh/°C) |
| $H^{OC}$ | Maximum height of OCWT (m) |
| $R_e^{ra}$ | Heat resistance factor between the common envelope of rooms r and ambient (°C /kW) |
| $R_e^{rr'}$ | Heat resistance factor between the common envelope of rooms r and r' (°C /kW) |
| $R_{ih}^r$ | Heat resistance factor between indoor temperature and heating system for room r (°C /kW) |
| $R_{ie}^r$ | Heat resistance factor between indoor temperature and wall for room r (°C/kW) |
| $R_w^{CC}$ | Heat resistance between the CCWT and the closet (°C/kW) |
| $\gamma^X$ | The weighting factor of market floors |
| $\theta_{In}^{OC}$ | The temperature of inlet water charged to OCWT (°C) |
| $\theta_W^{CC}$ | The closet temperature of the CCWT (°C) |
| $\theta_a$ | Ambient temperature (°C) |
| $\theta_{cl}^{CC}$ | The closet temperature of the CCWT (°C) |
| $\theta_{cl}^{OC}$ | The closet temperature of the OCWT (°C) |
| $\theta_i^{r,min/max}$ | Minimum/maximum indoor temperature for room r (°C) |
| $\theta_w^{z,min/max}$ | Minimum/maximum water temperature for OCWT and CCWT (°C) |
| $\kappa_w^r$ | The factor of incident solar irradiation for room r |
| $\lambda_t^{BM}$ | Balancing electricity price ($/kWh) |
| $\lambda_t^{DA}$ | Day-ahead electricity price ($/kWh) |
| $\lambda_t^{IM}$ | Intraday electricity price ($/kWh) |
| $\pi_{HP}^{up/down}$ | Ramp-up/-down rates of the compressor |
| $\rho_w$ | Specific heat value of water (J/Kg °C) |
| $\upsilon_{COP}$ | Coefficient performance of the heat pump |

*Variables*

| | |
|---|---|
| $\dot{m}_{CC}^r$ | Mass (water) flow of floor pipes for room r (kg/s) |
| $h_w^{OC}$ | Height of hot water in OCWT (m) |
| $\Pi_{DHW}^n$ | Heating power of DHW for consumer n (kW) |
| $\Pi_{HP}^{CC}$ | Heating power extracted from heat pump to supply CCWT (kW) |
| $\Pi_{HP}^{OC}$ | Heating power extracted from heat pump to supply OCWT (kW) |
| $\Pi_{HP}^{Total}$ | Total heating power consumption of the heat pump (kW) |
| $\Pi_R^r$ | Heating power extracted from heating system of room r (kW) |
| $\Pi_t^{BM}$ | Power trading in the balancing market (kW) |
| $\Pi_t^{DA}$ | Power purchase from the day-ahead market (kW) |
| $\Pi_t^E$ | Total power demand of the heat pump compressor (kW) |
| $\Pi_t^{IM}$ | Power trading in the intraday market (kW) |
| $\theta_h^r$ | The temperature of the heating system for room r (°C) |
| $\theta_F^{CC}$ | The water temperature of forward pipes for CCWT (°C) |
| $\theta_F^{OC}$ | The water temperature of forward pipes for OCWT (°C) |
| $\theta_R^{CC}$ | The water temperature of return pipes for CCWT (°C) |
| $\theta_W^{CC}$ | The water temperature of the CCWT (°C) |
| $\theta_W^{OC}$ | The water temperature of the OCWT (°C) |
| $\theta_e^r$ | The temperature of an envelope for room r (°C) |
| $\theta_i^r$ | The indoor air temperature for room r (°C) |

the power system imbalance [9].

In the residential sector, the penetration of heat pumps is increasing especially in countries with high RES penetration, e.g. Denmark [10], China [11], and Germany [12]. The heat pumps not only decrease the energy consumption cost but also facilitate the RES integration. Heat controllers play a crucial role in unlocking the flexibility potentials of heat pumps. From the energy viewpoint, the heat controllers have two distinct operation sides as follows:

1. Heating energy on the demand-side: Includes the thermal dynamics of buildings and thermal storage as well as the residents' comfort bounds.
2. Electrical energy on the supply-side: Includes the price data of the electricity markets and/or flexibility requirements of power systems.

Making a compromise between the two competing objectives, the controllers unlock the power-to-heat flexibilities. The operation of the controllers is strongly dependent on RES availability, energy price, occupancy pattern, and weather variables which are uncertain data. Therefore, the main motivation of the study is to design a heat controller closely aligned with uncertain electricity markets while addressing the uncertainties associated with weather variables and occupancy patterns.

### 1.2. Related studies

In the literature, the flexibility opportunities of heating systems stem from the following classifications:

1. Thermal inertia of mass and buildings [13].
2. Thermal storage devices [14].
3. Heat carriers [15].

The flexibility of thermal inertia of buildings refers to the storage capability of thermal masses, e.g. indoor temperature and envelopes

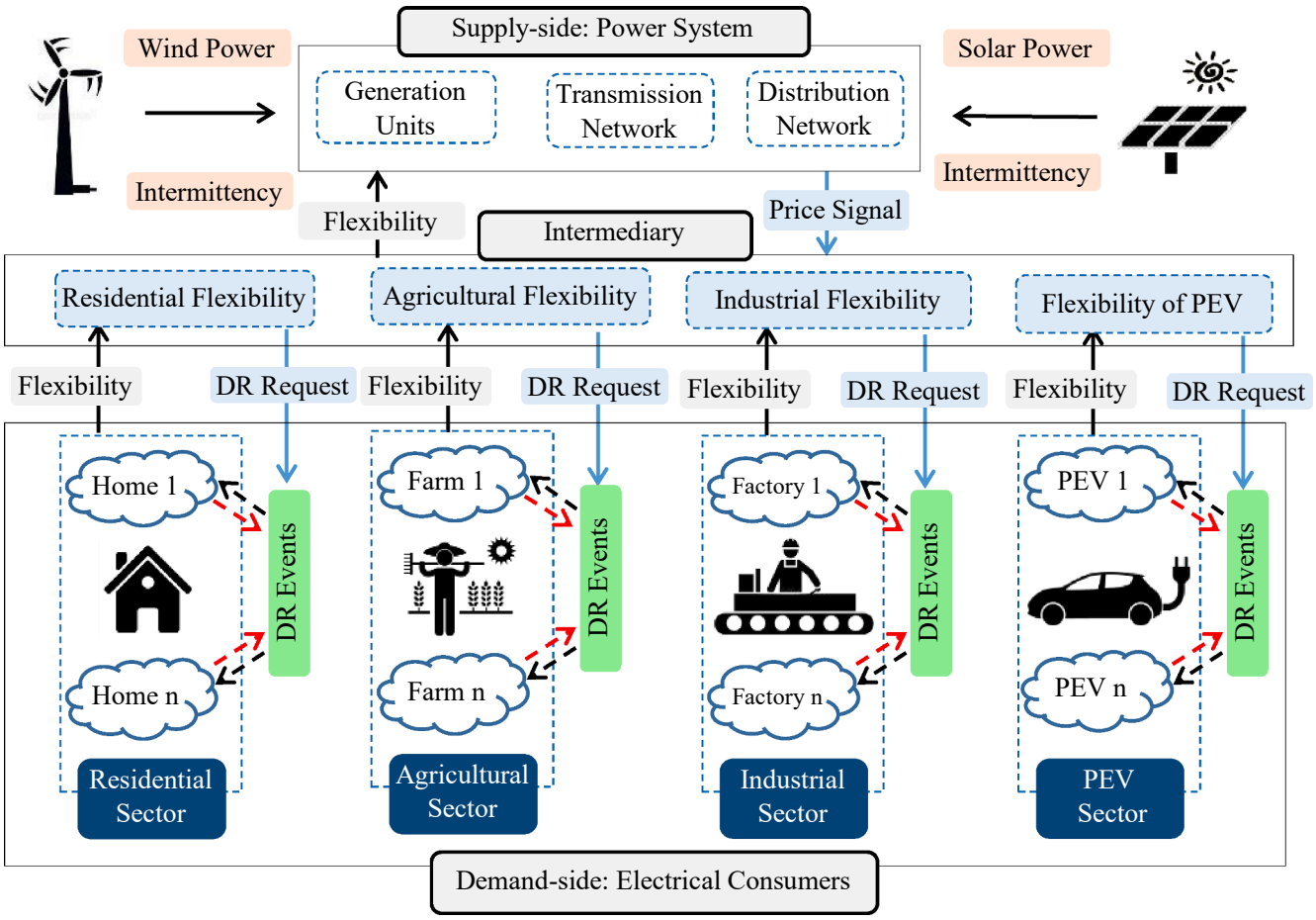


**Fig. 1.** Schematic diagram of demand-side flexibility in the power system topology.

[16]. This flexibility is shown by the thermal dynamics of the indoor temperature [17]. The indoor temperature satisfies the residents' comfort bound, including minimum and maximum comfort temperature. Adjusting the indoor temperature within the comfort bound, the thermal inertia flexibility is unlocked. In this way, the temperature is regulated in response to the flexibility requirements of the supply side. Therefore, when a RES shortage/excess happens in the power system, the controller sets the indoor temperature near the lower/upper thresholds [18]. The

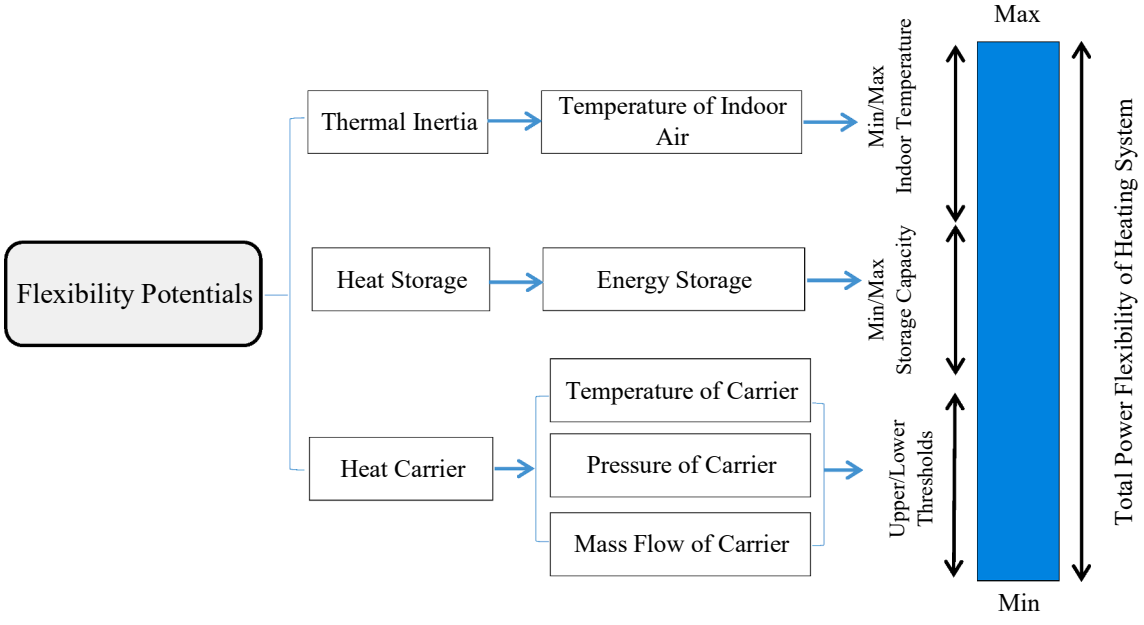


**Fig. 2.** Contribution of different flexibility potentials of heating systems.

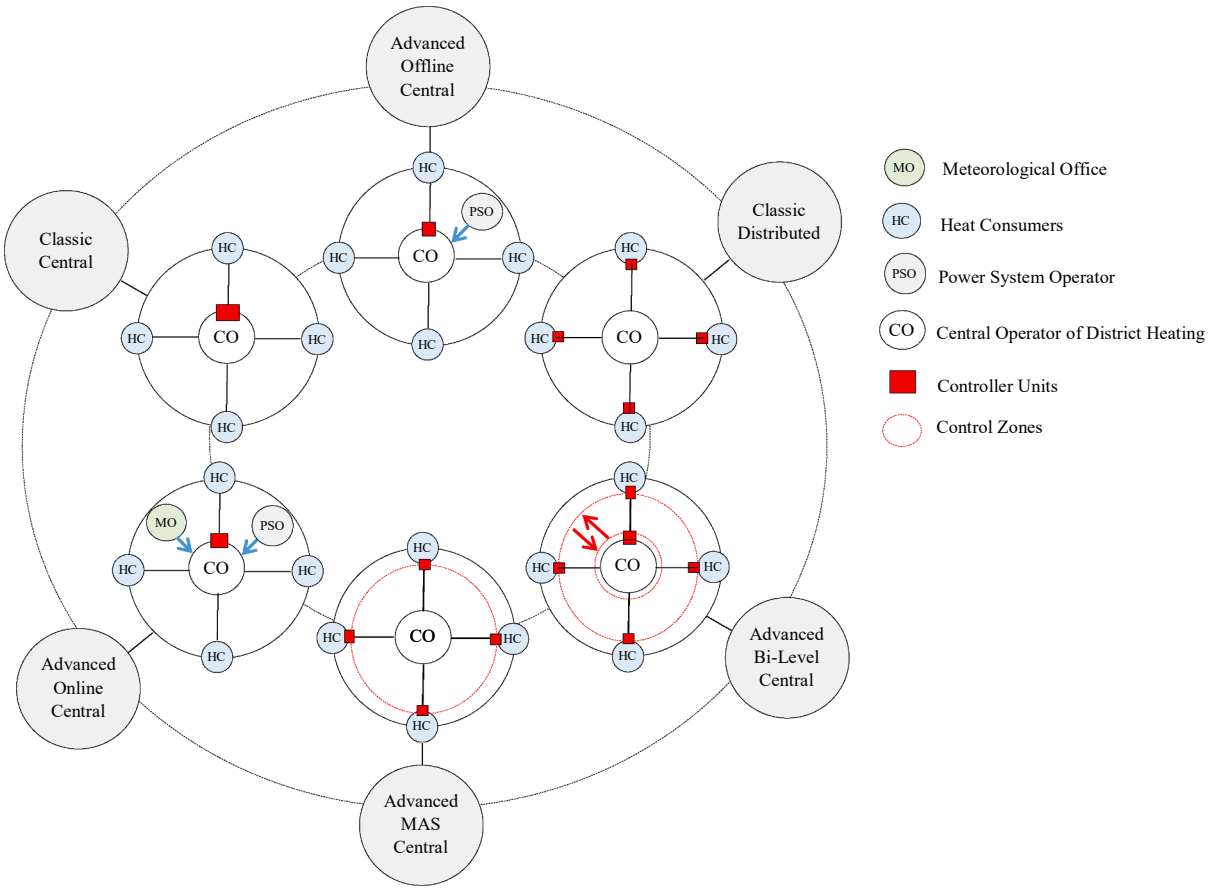


**Fig. 3.** Different generations of heat controllers in the literature.

value of this flexibility potential has a direct relation with the difference between the upper and lower thresholds [19].

The flexibility of thermal storage emanates from the devices which are especially devoted to heat flexibility [20]. Water tanks [21], chemical storages [22], aquifers [23], and boreholes [24] are the most conventional heat storage. The value of this flexibility potential is strongly dependent on the storage capacity of the equipment. In recent years, Phase Change Materials (PCM) have attracted much attention. PCMs are substances that absorb sufficient energy at the phase transition during the heating state and release the energy during the cooling process [25]. The PCMs are normally in two fundamental states of matter, including solid and liquid [26]. While the household water tanks provide power flexibility for short-term power markets, e.g. the day-ahead [27], adjustment [28], and real-time markets [29], the large-scale borehole storage provides long-term flexibility for seasonal markets [30].

The flexibility potential of the heat carrier is reflected in the storage capacity of the heat distribution network [31]. The thermal variables of the heating network, including carrier temperature, supply pressure, and mass flow are adjusted within a standard bound to provide heat flexibility. For example, the temperature of the heat carrier can be changed between 10 and 20 K to provide demand flexibility [32]. In this case, material fatigue [33] and pipe cracks [34] are possible failures, especially in join points. The flexibility of the heat carrier can be addressed in only the forward pipes and both forward and return pipes. In the former, the half content of the heat distribution network is addressed [35]. In the latter, the whole pipes are considered as the flexibility resource [32]. Fig. 2 describes how different flexibility potentials contribute to the total flexibility of heating systems.

To unlock the three types of flexibility potentials, heat controllers incorporate the flexibility requirements of the supply-side into the heating system. Generally, the heat controllers are stated in form of classic (conventional) and advanced (modern) controllers. The classic controllers refer to conventional controllers to provide a balance between supply and demand [36]. In these controllers, the technical requirements of the supply-side are not taken into account; therefore, the classic controllers normally fail to address demand-side flexibility. On the contrary, the advanced controllers aim to supply the heat demands addressing the technical requirements of the supply-side [37]. The control variables are normally addressed as heat demand, supply temperature, mass flow, and differential pressure [33]. Besides, the controllers are classified into centralized [38] or distributed [39]. Regarding the centralized controllers, the control variable is adjusted on the supply-side including the heating network or substations. In this case, supply temperature [40] and differential pressure [41] are the controllable variables. For the distributed controllers, the control variable is optimized on the demand side, e.g. buildings. In such controllers, heat demand [42] and mass flow [43] are the conventional control variables.

To unlock power-to-heat flexibility in response to power system requirements, the advanced controllers have communication with the supply side. From this viewpoint, the controllers are divided into offline and online controllers. The offline controllers incorporate the energy system requirements into the heating system in an offline mode [44]. The main drawback is that the controller operates the heating system based on predicted imperfect data, e.g. uncertain weather variables and electricity prices, which are subject to sensible variations. Approaching the energy delivery time, the operation of heating systems is mainly affected by uncertain climate variables, e.g. air temperature, wind speed, humidity, and solar irradiation [45]. To overcome this problem, the online controllers are suggested to adjust the operation of the heating system based on the updated data of uncertain variables.

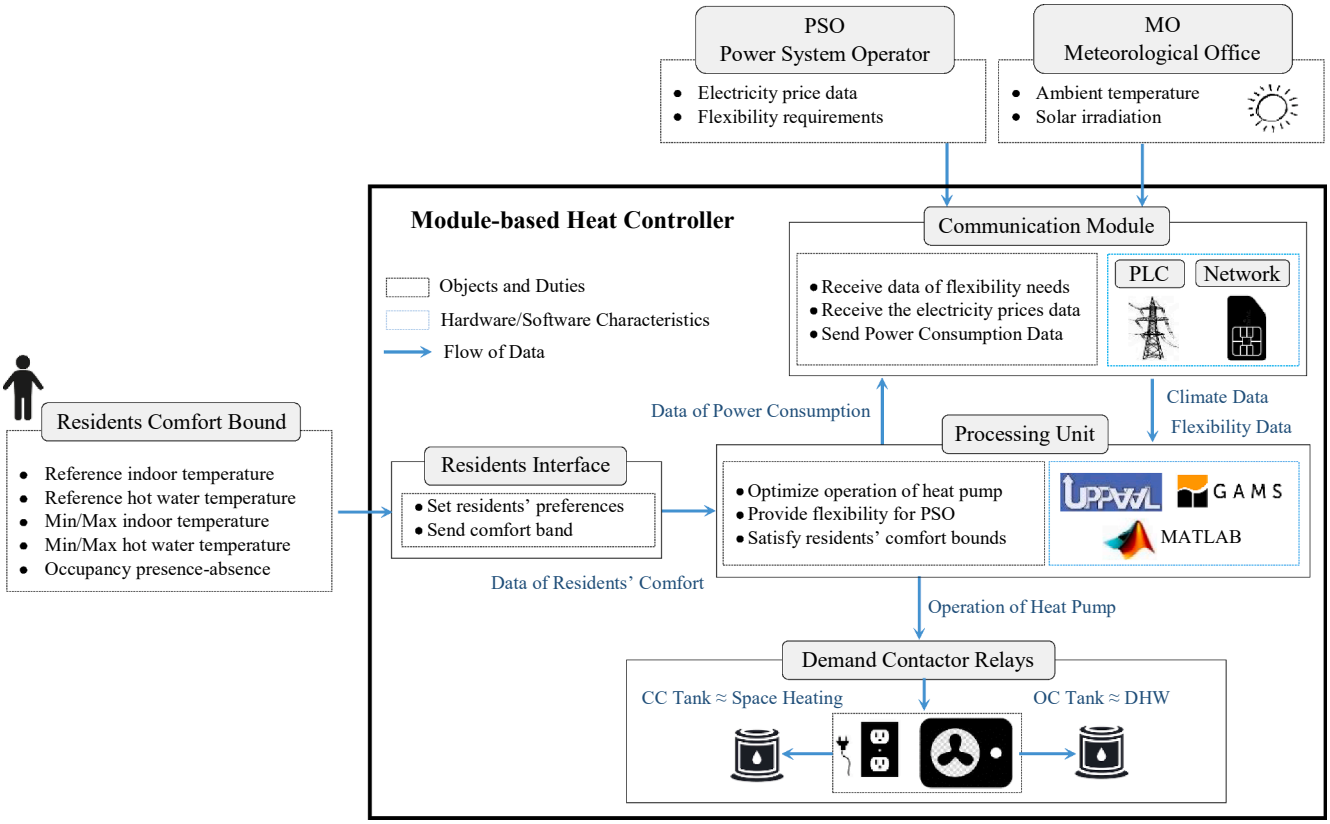


**Fig. 4.** Schematic structure of the heat controller.

Recently, Model Predictive Control (MPC) [46], Economic MPC (EMPC) [47], and Multi-agent Systems (MAS) [48] are highly emphasized in this regard. To sum up, the different generations of heat controllers are depicted in Fig. 3.

### 1.3. Paper contributions

In this paper, a heat controller is designed with a three-stage stochastic objective function. The stages of the stochastic function are associated with the trading floors of electricity markets with high RES penetration, e.g. Nordic Electricity Market. The controller addresses the EMPC approach to adjust the energy consumption in three market floors including the day-ahead, intraday, and balancing markets from 24 h before power delivery time until real-time. At the same time, the controller updates the weather data, e.g. ambient temperature. Having communication with Meteorological Office (MO) and Power System Operator (PSO), the controller optimizes the heat consumption to provide demand flexibility for the power system. The heat controller supplies both space heating and Domestic Hot Water (DHW) consumption. Regarding space heating, the thermal dynamics of the buildings are developed to discuss different temperature zones based on occupancy patterns. The main contributions of the paper can be stated as follows:

1. Suggesting stochastic EMPC to adjust heat consumption on long, mid, and short advance notices of RES availability.
2. Unlocking flexibility potentials of space heating and DHW consumption by closed-cycle and open-cycle water tanks.
3. Studying the impacts of uncertain electricity price, ambient temperature, and DHW consumption on the operation of the heating system.

The rest of the paper is organized as follows. In Section 2, the problem methodology is described. Section 3 illustrates the mathematical formulations of the problem. In Section 4, the numerical studies, simulations, and discussions are presented. Section 5 concludes the suggested approach.

## 2. Problem methodology

This study designs a demand controller for heat consumption of residential buildings including space heating and DHW. The heating system is supplied by an electric heat pump. The controller accepts input data from the supply-side and demand-side. On the supply side, the controller has communication with PSO and MO to receive the flexibility requirements and climate data, respectively. On the demand side, the residents set their desired comfort bound into the controller.

The controller is supplied by a power system with high RES penetration. Therefore, it aims to provide power-to-heat flexibility for the upstream network based on RES availability. The controller integrates flexibility opportunities of the heating system into the three markets on 24 h-ahead, 1 h-ahead, and a few seconds-ahead on long, mid, and short notices, respectively.

On the supply side, RES availability has a close correlation with the electricity price. Therefore, the uncertain prices of the three market floors are reflective of the RES intermittency. To model the price uncertainties, Auto-Regressive Integrated Moving Average (ARIMA) is addressed as the scenario generation approach. The uncertainty of climate data, i.e. the ambient temperature, as well as the DHW consumption is modeled as envelope bounds with minimum and maximum deviations.

To optimize the competing objectives under severe uncertainties, three-stage stochastic programming is embedded in the objective function of the controller. The suggested approach uses the MPC control technique in which enables the controller to optimize the current timeslots while anticipating future events and take control actions accordingly. To minimize the energy consumption cost, the objective

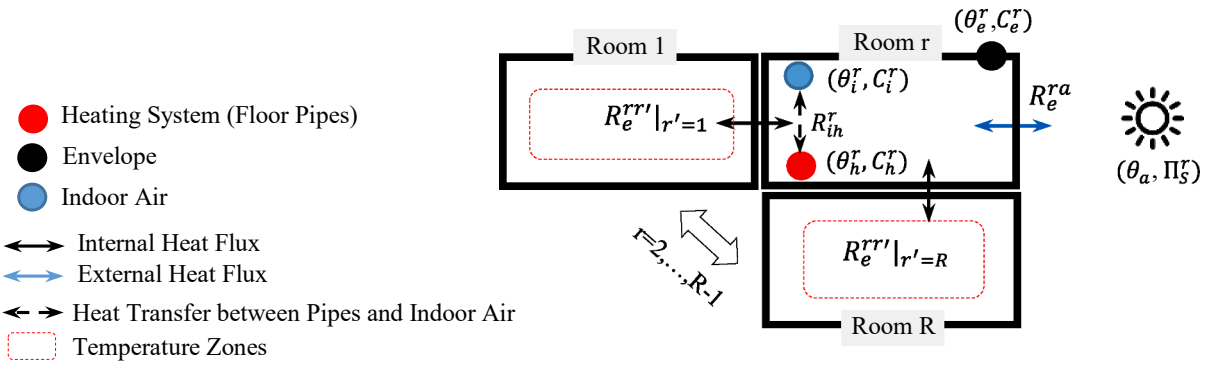


**Fig. 5.** Diagram of the thermal dynamics of buildings.

function uses economic terms of the electricity market. As a result, the controller is called Stochastic Economic Model Predictive Control (SEMPC).

The MPC relies on the thermal dynamics of the buildings which are obtained by model identification. To identify the thermal dynamics of the building, the measurement data, i.e. indoor air temperature, ambient temperature, solar irradiation, and heating consumption, are imported to the model identification. Continuous-Time Stochastic Model (CTSM) is used to estimate the thermal dynamics. The CTSM is run for 5 days' worth of sensor data. The MPC is trained by the CTSM to embed the thermal dynamics of the buildings into the controller. Finally, the controller optimizes the heating demand of the building based on RES availability and climate variables while meeting the residents' comfort bounds.

To provide a general insight into the issue, Fig. 4 depicts the schematic diagram of the controller. As the figure reveals, the controller is suggested in a module-based structure to show the communication, processing, user interface, and relay units clearly. The control algorithm is coded in the processing unit. In this unit, different software tools, e.g. UPPAAL [49], GAMS [50], and MATLAB [51], can be adopted.

## 3. Problem formulations

In this section, the main structures of the problem are formulated mathematically. To clarify the suggested approach, the problem is presented in different subsections.

### 3.1. Model identification

To unlock the flexibility opportunities of thermal inertia, the thermal dynamic behavior of the buildings should be investigated. The residential buildings are comprised of rooms, including kitchens, living rooms, bedrooms, and bathrooms, with different temperature needs. To provide power flexibility, the operation of the heating systems is optimized based on the occupancy presence and absence in rooms. In this way, despite the reduction of energy consumption cost, the power system takes the advantage of demand flexibility. To achieve the aim, different temperature zones are defined in rooms based on temperature needs and occupancy patterns. From the viewpoint of thermal dynamics, the heat flux between the adjacent rooms must be addressed in addition to the conventional heat exchange with external envelopes. Therefore, the thermal dynamics of the residential building with R rooms are formulated as follows [52]:

$$\frac{d\theta_i^r(t)}{dt} = \frac{1}{C_i^r} \times \left( \frac{(\theta_h^r(t) - \theta_i^r(t))}{R_{ih}^r} + \frac{(\theta_e^r(t) - \theta_i^r(t))}{R_{ie}^r} + (\kappa_w^r \times \Pi_S^r(t)) + \sigma_i d\omega_i \right) \tag{1}$$

$$\frac{d\theta_e^r(t)}{dt} = \frac{1}{C_e^r} \times \left( \frac{(\theta_i^r(t) - \theta_e^r(t))}{R_{ie}^r} + \sum_{\substack{r'=1 \\ r' \neq r}}^{R} \frac{(\theta_i^{r'}(t) - \theta_e^r(t))}{R_e^{rr'}} + \sum_{a=1}^{A} \frac{(\theta_a(t) - \theta_e^r(t))}{R_e^{ra}} + \sigma_e d\omega_e \right) \tag{2}$$

$$\frac{d\theta_h^r(t)}{dt} = \frac{1}{C_h^r} \times \left( \frac{(\theta_i^r(t) - \theta_h^r(t))}{R_{ih}^r} + \Pi_R^r(t) + \sigma_h d\omega_h \right) \tag{3}$$

Let consider a building with R rooms. The set of differential equations explain the thermal dynamics for room r. Eq. (1) shows the thermal dynamics of the indoor temperature. The first and second terms indicate the heat transfer between the floor pipes and indoor temperature, and between indoor air and envelopes, respectively. The third term describes the heating power captured from solar radiation. Eq. (2) illustrates the thermal dynamics of the envelope temperature. In this model, the first term explains the heat exchange between the indoor air of room r and its envelopes. The second term states the heat flux between the envelopes of room r and the indoor air of rooms r'. This term describes the heat flux between the room r with the surrounded rooms r'. The third term expresses the heat flux between the envelopes of room r and ambient temperature. This term is related to envelopes surrounded by ambient (unconditioned environment). Eq. (3) explains the thermal dynamics of the floor pipes. The first term discusses the heat transfer between the floor pipes and indoor air. The second term shows the heating power of the floor pipes. Note that the heating systems of rooms are in the form of floor pipes. Fig. 5 describes the thermal dynamics of the suggested approach with a schematic diagram.

In this model, the last terms of the equations, i.e. the blue color terms, indicate the standard Wiener process $\omega_x$, x∈{i,e,h} with the incremental variance $\sigma_x^2$ [53,54]. In the thermal dynamics, the constant coefficients $R_x$, $C_x$, $\kappa_w$ depend on the physical characteristics of the building, e.g. envelope materials and quality of insulation. To estimate the coefficients, the CTSM links a data-driven approach with the thermal dynamics. The approach uses the measurement data to estimate the constant parameters of the thermal dynamics. The sensor data includes indoor temperature, ambient temperature, solar irradiation power, and heating consumption ($\theta_i$,$\theta_a$,$\Pi_S$,$\Pi_R$) which are extracted from measurement sensors. Let formulate the sensor data such that:

$$Y_k = T_{ik} + e_k \tag{4}$$

where $t_k$ describes the time slot of a data measurement at point k; $Y_k$ states the sensor data, and $e_k$ denotes the measurement error as Gaussian

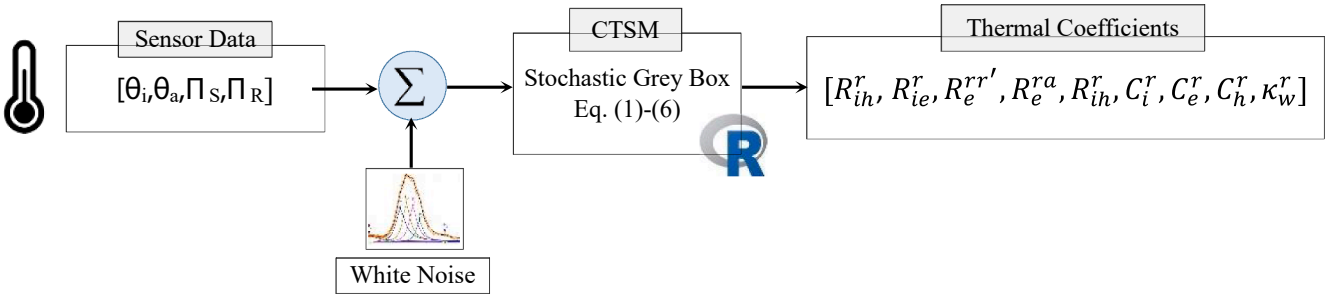


**Fig. 6.** Stochastic grey box of CTSM.

white noise. The sensor data are $[\theta_i,\theta_a,\Pi_S,\Pi_R]$.

Given the measurement input data, the maximum likelihood estimation of parameters, including $\left[C_i^r, C_e^r, C_h^r, R_{ih}^r, R_{ie}^r, R_e^{rr'}, R_e^{ra}, R_{ih}^r, \kappa_w^r\right]$, are obtained. Training the model with the sensor data, the maximum likelihood is described mathematically as follows [53]:

$$L(\theta, Y_N) = \left(\prod_{k=1}^{N} p(Y_k|Y_{k-1},\theta)\right) p_0(Y_0|\theta) \tag{5}$$

$$\theta^s = argmax[L(\theta; Y_N)] \tag{6}$$

The operator p(.) denotes a conditional density while observing the sensor data at point *k*, previous point *k-1* and the target variable θ. Also, the initial conditions are shown with $p_0(.)$. Consequently, Eq. (6) matches the maximum likelihood for the target variable $\theta^s$. The CTSM is developed by the Department of Computer Science, DTU, Denmark, using statistical language R. The software is publicly available at [55]. Besides, instructions and tutorial files are available at [53]. Fig. 6 depicts the schematic of the stochastic gray box in the CTSM approach.

### 3.2. Thermal storage

The heat pump supplies the heat energy of both the space heating and the DHW. In this way, two water tanks are addressed as Closed-Cycle Water Tank (CCWT) and Open-Cycle Water Tank (OCWT). The CCWT supplies the heat demand of the floor pipes. The volume of water remains unchanged in the forward and return pipes. The OCWT supplies the DHW consumption in the kitchen and bathroom. Therefore, there is no return pipe for the OCWT. Instead, the water tank is refilled with inlet water from the water distribution system.

The thermal dynamics of the CCWT are stated as follows:

$$\frac{d\theta_w^{CC}(t)}{dt} = \frac{1}{C_w^{CC}} \times \left(\Pi_{HP}^{CC}(t) - \sum_{r=1}^{R} \Pi_R^r(t) + \frac{(\theta_{Cl}^{CC}(t) - \theta_w^{CC}(t))}{R_w^{CC}}\right) \tag{7}$$

$$\Pi_R^r(t) = \dot{m}_{CC}^r(t) \times \rho_w \times (\theta_F^{CC}(t) - \theta_{R,r}^{CC}(t)) \tag{8}$$

Eq. (7) describes the variations of the water temperature for consecutive times. The first right term shows the power consumption; the second term states the summation of heat consumption for R rooms and the third term explains the thermal loss from the tank shell. Eq. (8) expresses the heat consumption of room r as a function of mass flow and water temperature of forward/return pipes. Despite the heat loss in water pipes, the forward water temperature is normally equal to the water temperature of the water tank $\theta_F^{CC} \approx \theta_w^{CC}$.

As mentioned above, the main difference between the CCWT and OCWT is that the volume of the water in the CCWT maintains the same level due to the return water from floor pipes. In contrast, there is no return pipe in the OCWT where the tank is refilled by the fresh inlet water. Therefore, the thermal dynamics of the OCWT are formulated as follows:

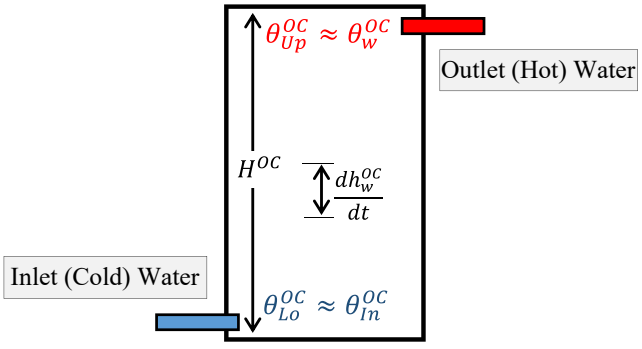


**Fig. 7.** The OCWT with inlet and outlet temperatures.

$$\frac{d\theta_w^{OC}(t)}{dt} = \frac{1}{C_w^{OC}} \times \left(\Pi_{HP}^{OC}(t) - \sum_{n=1}^{N} \Pi_{DHW}^n(t) + \frac{(\theta_{Cl}^{OC}(t) - \theta_w^{OC}(t))}{R_w^{OC}}\right) \tag{9}$$

$$\Pi_{DHW}^n(t) = \dot{m}_{DHW}^n(t) \times \rho_w \times (\theta_F^{OC}(t) - \theta_{In}^{OC}(t)) \tag{10}$$

In the same way, Eq. (9) denotes the variation of water temperature for the OCWT. The second right term describes the heat consumption of DHW in room n. Generally, in a residential building, the DHW is consumed in the kitchen and bathroom $n \in r, N \ll R$. Eq. (10) shows the heat consumption of DHW in room n.

To evaluate the volume of water in the OCWT, a two-mass composite model is addressed. The approach considers two water segments including upper and lower segments. The upper segment has a uniform temperature close to the forward water to the DHW consumers. The lower segment is reflective of a uniform temperature of the inlet water from the water distribution system. The model is used to calculate the height of hot water in the OCWT during the operation. The following equations describe the height variation of hot water in the OCWT [56]:

$$\frac{dh_w^{OC}}{dt} = \alpha^{OC} - \left(\beta^{OC} \times h_w^{OC}\right) \tag{11}$$

$$\alpha^{OC} = \left(H^{OC} \times \frac{\Pi_{HP}^{OC} + \frac{(\theta_{Cl}^{OC} - \theta_{Lo}^{OC})}{R_w^{OC}}}{C_w^{OC} \times (\theta_{Up}^{OC} - \theta_{Lo}^{OC})}\right) - \left(\frac{H^{OC} \times \dot{m}_{DHW}^n \times \rho_w}{C_w^{OC}}\right) \tag{12}$$

$$\beta^{OC} = \frac{1}{C_w^{OC} \times R_w^{OC}} \tag{13}$$

In the two-mass composite model, the water temperatures for the upper and lower segments are equal to hot water temperature and inlet water temperature, $\theta_{Up}^{OC} \approx \theta_w^{OC}$ and $\theta_{Lo}^{OC} \approx \theta_{In}^{OC}$.

Fig. 7 illustrates the structure of the OCWT with inlet and outlet water pipes.

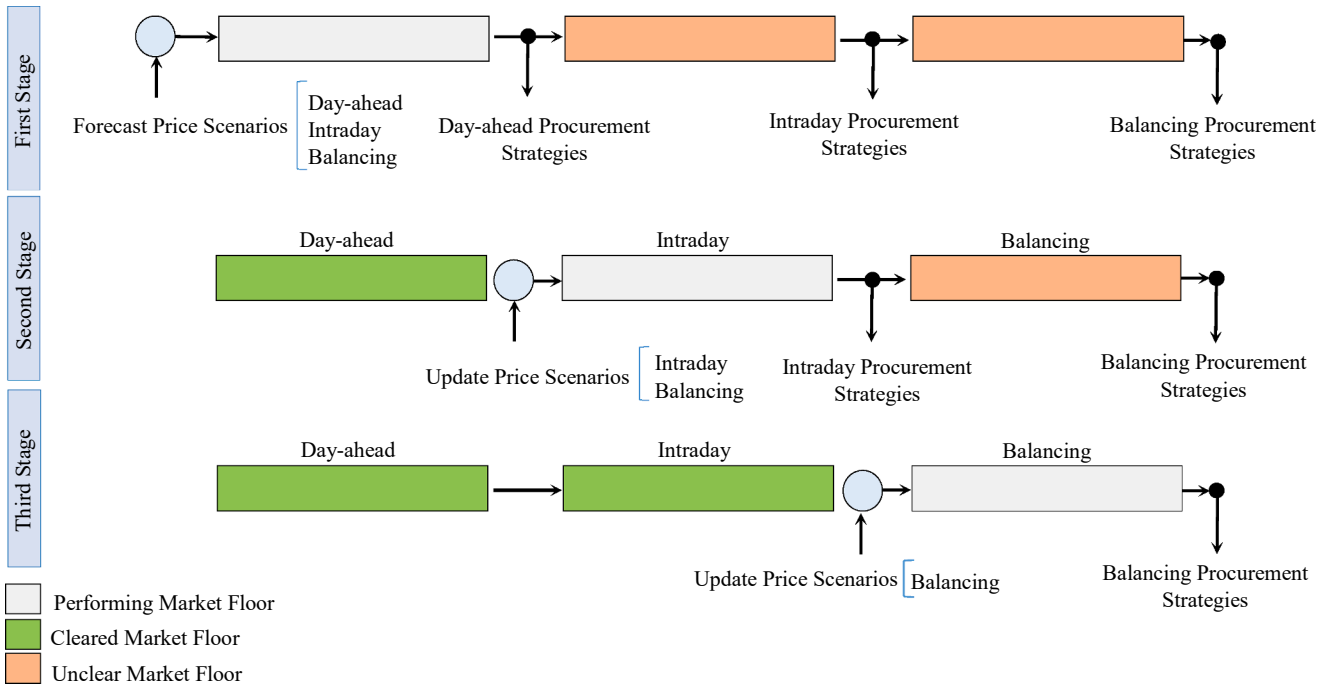


**Fig. 8.** Market performance in the three-stage stochastic programming.

### 3.3. Stochastic economic model predictive control

The heat controller aims to minimize the heat consumption cost of the household in terms of space heating and DHW consumption attaining the following key objectives:

1. Providing demand flexibility for power systems.
2. Minimizing power consumption cost of households.
3. Satisfying the residents' comfort bounds.

To fulfill the first objective, the controller procures the required power from three trading floors of electricity markets. The controller optimizes the heat consumption in response to flexibility requirements of the supply-side from 24 h ahead in the day-ahead market until real-time in the balancing market. To attain the second objective, an economic objective is embedded into the controller to minimize the energy consumption cost of the household. The objective function includes the electricity prices of the three market floors. Finally, to meet the third objective, the residents' comfort bounds are set to the controller by occupants. The comfort bounds are set to the controller as the constraints of the optimization approach.

The three market floors are modeled through three-stage stochastic programming as follows [52]:

$$F^{FirstStage} = \underset{\left(\Pi_t^{DA}(\omega)\right)}{Minimize}\left(\sum_{\omega\in N_\omega}\sum_{t=\tau}^{N_\tau} \mathrm{E}_{\omega_1}\left[\lambda_t^{DA}(\omega_1)\times\Pi_t^{DA}(\omega_1)+F^{SecondStage}\right]\right) \tag{14}$$

$$F^{SecondStage} = \underset{\left(\lambda_t^{IM}(\omega_2)\right)}{Minimize}\left(\sum_{\omega\in N_\omega}\sum_{t=\tau}^{N_\tau} \mathrm{E}_{\omega_2|\omega_1}\left[\lambda_t^{IM}(\omega_2)\times\Pi_t^{IM}(\omega_2)+F^{ThirdStage}\right]\right) \tag{15}$$

$$F^{ThirdStage} = \underset{\left(\Pi_t^{BM(+)}(\omega),\Pi_t^{BM(-)}(\omega)\right)}{Minimize}\left(\sum_{\omega\in N_\omega}\sum_{t=\tau}^{N_\tau}\left[\mathrm{E}_{\omega_3|\omega_1,\omega_2}\left[\left(\lambda_t^{BM(+)}(\omega_3)\times\Pi_t^{BM(+)}(\omega_3)\right)-\left(\lambda_t^{BM(-)}(\omega_3)\times\Pi_t^{BM(-)}(\omega_3)\right)\right]\right]\right) \tag{16}$$

where Index $E$ denotes the expectation function. The objective function is stated in three stages. In the first stage, the controller can purchase $\gamma^{DA}$ % of the required power from the day-ahead market. The day-ahead market is performed 24 h before power delivery time. The day-ahead electricity price includes informative data about power availability in the electricity market. Therefore, the controller optimizes the energy consumption for the next 24 h on long advance notice of power flexibility. Eq. (14) states the objective function of the first stage in the day-ahead market.

Afterward, the intraday market is cleared 60–10 min prior to power delivery time. In the second term, the controller is allowed to purchase/sell power from/to the intraday market. In cases when the intraday market experiences a power deficit, the intraday price increases. In response, the controller may decide to sell a part of the day-ahead purchased power to the intraday market not only to provide flexibility for the electricity market but also to make a profit. Adversely, the controller can purchase power from the intraday market at low price hours when the market faces power excess. The controller can trade (buy/sell) $\gamma^{ID}$ % of the required power in the intraday market to provide power flexibility on mid advance notice. Eq. (15) describes the objective function of the second stage in the intraday market.

Finally, the third term indicates the power trading in the balancing market which is performed a few seconds before power delivery time. The controller can trade (buy/sell) $\gamma^{BM}$ % of the required energy in the balancing market to provide up-/down-regulation at the opposite side of the power system imbalance. The controller purchases power from the market at low price hours when the market faces power excess, i.e. positive system imbalance. In contrast, the controller sells a part of the day-ahead/intraday purchased power to the balancing market in high price hours when the power system experiences a severe power

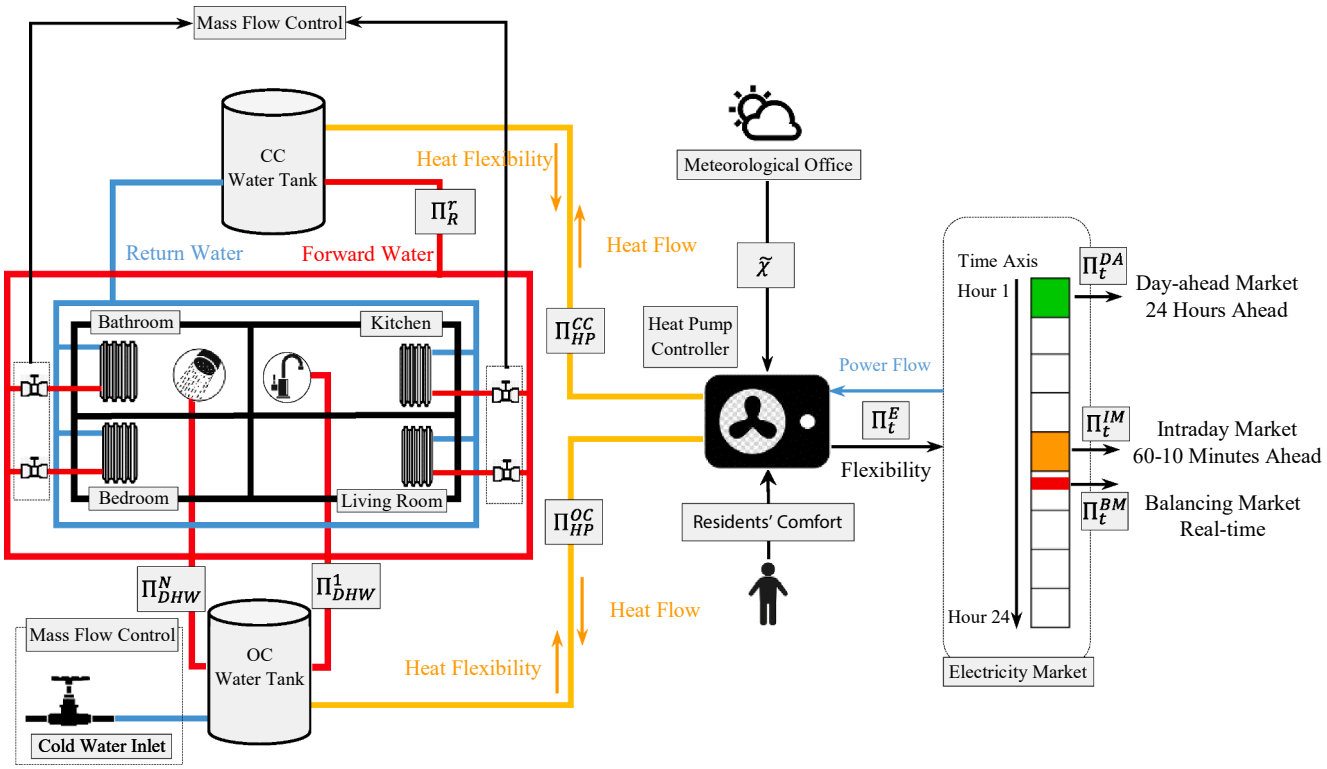


**Fig. 9.** Energy paradigm of the suggested heating system in terms of heat and power.

shortage, i.e. the negative power system imbalance. Therefore, the controller provides power flexibility for the supply-side on short advance notice. Note that superscripts +/- denote the positive and negative states of power system imbalances. Eq. (16) explains the objective function of the third stage in the balancing market.

The power procurements from the three market floors are optimized in three stages of price forecasting. In the first stage, the day-ahead, intraday, and balancing market prices are forecasted 24 h before energy delivery time. Approaching power delivery time, the price uncertainties decrease. Therefore, after performing the day-ahead market, the price scenarios of intraday and balancing markets are updated in the second stage. In the same way, the price scenarios of the balancing market are updated in the third stage before performing the balancing market. Fig. 8 explains how the three stages of stochastic programming and price forecasting work.

- **Supply-side Constraints**

The supply-side constraints ensure the participation of the controller in the market floors to provide structural flexibility for the power system as well as energy cost minimization for the households. The constraints can be stated as follows [52]:

$$0 \leqslant \Pi_t^{DA}(\omega_1) \leqslant \gamma^{DA} \times \Pi_t^{Rated} \tag{17}$$

$$\left|\Pi_t^{IM}(\omega_2)\right| \leqslant \gamma^{IM} \times \Pi_t^{Rated} \tag{18}$$

$$\left|\Pi_t^{BM}(\omega_3)\right| \leqslant \gamma^{BM} \times \Pi_t^{Rated} \tag{19}$$

$$\sum_{x \in X} \gamma^x = 1,\ X = \{DA, IM, BM\} \tag{20}$$

$$\Pi_t^{E}(\omega) = \Pi_t^{DA}(\omega_1) + \Pi_t^{IM}(\omega_2) + \Pi_t^{BM}(\omega_3) \tag{21}$$

$$\Pi_t^{DA}(\omega_1) + \Pi_t^{IM}(\omega_2) \geqslant 0 \tag{22}$$

Eq. (17) enforces that the controller can purchase $\gamma^{DA}$ % of the required power from the day-ahead market. Besides, it cannot sell power to this market floor. In the same way, Eqs. (18) and (19) state that the controller trades (purchases/sells) $\gamma^{IM}$ % and $\gamma^{BM}$ % of the nominal power in the intraday and balancing markets, respectively. The market coefficients $\gamma^x$ confines the power trading capacity of the controller to a fraction of the rated electricity consumption of the heat pump compressor. The reason is that the controller can buy a considerable value of power from the day-ahead market to sell in the balancing market with higher prices. These measures may exercise market power and cause market speculation. To overcome the problem, constraint (20) limits the total power trading of the controller to the nominal power consumption of the heating system. Eq. (21) shows the power balance equation. Finally, Eq. (22) ensures that the amount of sold energy to the intraday market is less than the purchased power from the day-ahead market.

Worth mentioning that the single apartment blocks, as well as any small-scale electricity consumers, cannot take part in wholesale electricity markets directly. To make it possible, the demand response provider and/or district heating aggregators integrate the demand flexibility of a significant number of heat consumers into power systems. The district heating aggregators are intermediary agents to take part in the wholesale market on behalf of the end-users.

The market coefficients should be organized in descending order from the day-ahead to the balancing market $\gamma^{DA} > \gamma^{IM} > \gamma^{BM}$. In daily electricity markets, the balancing market is much more volatile than the day-ahead market. Therefore, a demand spike in the balancing market may cause price instability. Besides, the real-time markets aim to provide power regulation instead of profit-making. For these reasons, the capacity of power trading in the balancing market should be confined to prevent speculating.

- **Demand-side Constraints**

The demand-side constraints guarantee the residents' comfort

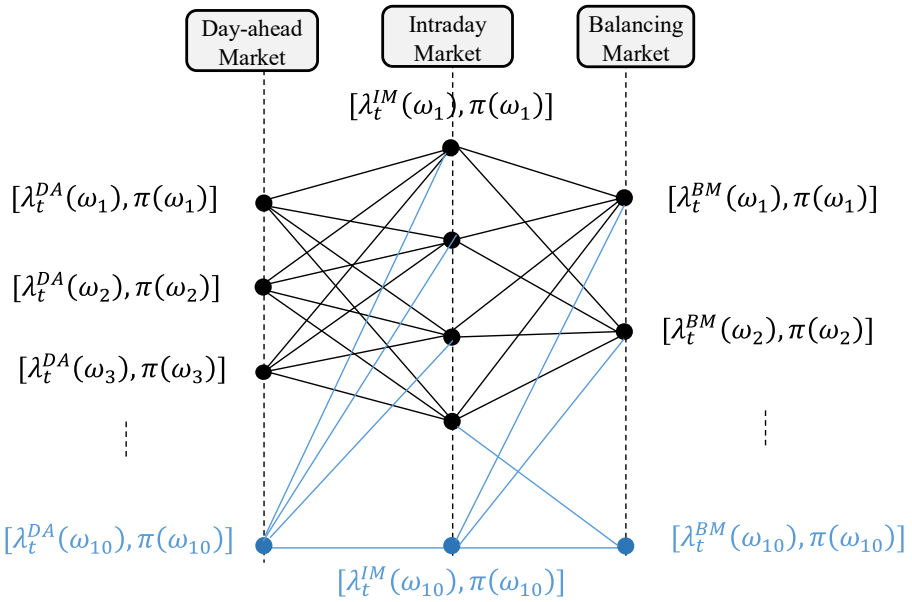


**Fig. 10.** Scenario graph for electricity prices, including 10 scenarios for each market floor.

bounds as well as the optimum operation of the heating system. The constraints are described as follows:

$$\theta_i^{r,min} \leqslant \theta_i^r(t) \leqslant \theta_i^{r,max} \tag{23}$$

$$\theta_w^{Z,min} \leqslant \theta_w^Z(t) \leqslant \theta_w^{Z,max} \quad , Z = \{CC, OC\} \tag{24}$$

$$\Pi_t^E = \frac{\Pi_{HP}^{Total}}{\vartheta_{COP}} = \frac{(\Pi_{HP}^{OC} + \Pi_{HP}^{CC})}{\vartheta_{COP}} \tag{25}$$

$$\Pi_t^E - \Pi_{t-1}^E \leqslant \pi_{HP}^{up} \tag{26}$$

$$\Pi_{t-1}^E - \Pi_t^E \leqslant \pi_{HP}^{down} \tag{27}$$

Eqs. (23) and (24) describe the residents' comfort bounds for temperatures of indoor air and water tanks. The flexibility potentials of the heat controller mainly depend on the maximum/minimum occupants' comfort temperature. Eq. (25) states the electricity consumption of the heat pump compressor as a function of the heat consumption of CCWT and OCWT. The ramp-up/-down rates of the heat pump compressor are shown by (26) and (27).

To sum up, Fig. 9 depicts the energy diagram of the suggested heating system in terms of power-heat flow. Note that the control variables for the CCWT and OCWT are $\dot{m}_{CC}^r$and $\dot{m}_{DHW}$, respectively. In the space heating, the controller adjusts the water flow to the radiators through the mass flow valves. In the DHW, the water flow from the cold water inlet is controlled to fulfill the optimum temperatures. Therefore, the controller adjusts the mass flow of four valves in the four rooms and one valve of the inlet water. To clarify, the control valves are pointed out in this figure.

### 3.4. Uncertainty characterization

The controller optimizes the operation of the heating system for the next 24 h. The heat pump operation is mainly dependent on stochastic variables with imperfect data. On the supply side, the electricity price is the key uncertain variable that affects the operation of the heat pump. On the demand side, the uncertain behavior of the residents, e.g. DHW consumption, may change the heat pump operation. Besides, the thermal dynamics of the buildings are affected by uncertain climate data, including ambient temperature and solar irradiation. Therefore, in practice, the controller is confronted with uncertain electricity prices, weather data, and residents' behavior.

First of all, to model the electricity price uncertainties, the ARIMA approach is used. The ARIMA is fitted to time series data to forecast future points. The controller uses historical market data to forecast the electricity price for the next 24 h. The ARIMA model can be stated as the following time series:

$$\lambda_t = (\alpha) + \left(\beta_1\lambda_{t-1} + \beta_2\lambda_{t-2} + \ldots + \beta_p\lambda_{t-p}\right) + \left(\phi_1\varepsilon_{t-1} + \phi_2\varepsilon_{t-2} + \ldots + \phi_q\varepsilon_{t-q}\right) \tag{28}$$

The time series (28) describes how the electricity price is predicted using historical data. In this model, the predicted price is comprised of three terms. The first term is a constant. The second term is the linear combination of $p$ lags of predicted price. The third term shows the $q$ lagged forecast errors. Therefore, the ARIMA is used to generate scenarios for the day-ahead, intraday, and balancing market prices. The scenarios are generated with associated probabilities in which the summation of the probabilities for each time slot is equal to one.

In this study, 10 price scenarios are generated on each market floor for each time slot (hour). It means that the day-ahead market has 24 × 10 scenarios during the daily operation. In the same way, 10 scenarios are generated for the intraday and balancing markets at each time slot. Therefore, the total number of price scenarios for the three market floors at each time slot is equal to $10^3$. Fig. 10 illustrates the scenario graph of the three electricity markets. Let consider x = {DA,IM,BM} as the index of electricity markets. Then, the electricity market scenario is introduced by an electricity price value $\lambda_t^x(\omega)$ and the associated probability $\pi(\omega)$. Note that the summation of scenario probabilities at each time slot is equal to 1 as $\sum_{i=1}^{10}\pi(\omega_i) = 1$.

To model the imperfect data of the climate variables, i.e. ambient temperature, as well as the DHW consumption, an envelope bound is addressed. The envelope bound is comprised of a nominal value, i.e. the predicted data, and positive/negative deviations. The initial operation of the heating system is optimized based on the expected value of the uncertain electricity prices and nominal values of weather variables. The upper and lower thresholds of the envelope bound describe the possible deviations of the uncertain variables. To study the impacts of the uncertain data on the heating system operation, the whole interval of the envelope bound is split into N subintervals. The electricity consumption of the heat pump is firstly scheduled, then is adjusted, and finally is regulated in the three market floors based on the deviation bounds of the uncertain variables.

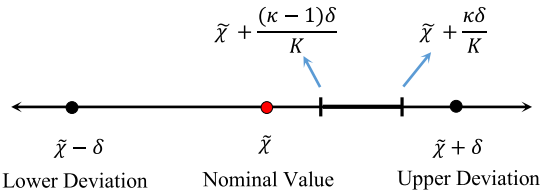


**Fig. 11.** Envelope bound for variables with imperfect data.

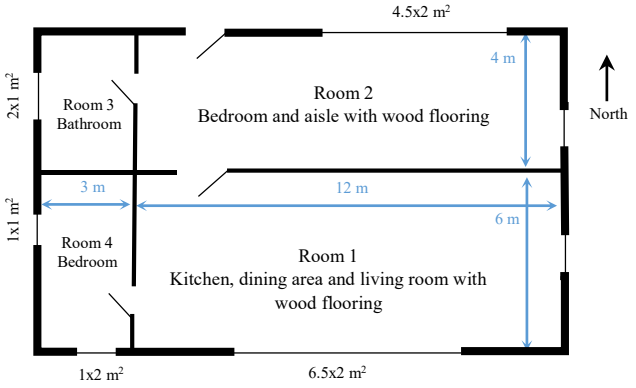


**Fig. 12.** The 150 $m^2$ Danish test house with 4 rooms [51].

The envelope bound is divided into subintervals using the following steps:

**Step 1:** Construct the envelope bound of the uncertain data as follows:

$$\chi = [\chi^{min}, \chi^{max}] = [\widetilde{\chi}-\delta, \widetilde{\chi}+\delta] \tag{29}$$

**Step 2:** Split the envelope bound $\chi$ into K subintervals subject to:

$$\chi(\kappa) = \left\{ \begin{array}{ll} \chi \in R_+, & \forall \chi \in \left[\widetilde{\chi}+\frac{(\kappa-1)\delta}{K}, \widetilde{\chi}+\frac{\kappa\delta}{K}\right] \\ \forall \kappa = 1, ..., K: & \chi^{\kappa} = \kappa \times \frac{|\chi^{max}-\chi^{min}|}{K} \end{array} \right\} \tag{30}$$

where $\chi$ denotes the uncertain data; $\delta$ is the maximum deviation; $\kappa$ shows the counter index of the subintervals.

Finally, Fig. 11 depicts the structure of the envelope bound.

## 4. Numerical studies

In this section, the suggested approach is examined on a test house with sensor data. Besides, the price data from the Danish sector of the Nordic Electricity Market is used. The MPC and CTSM are coded in MATLAB and language R, respectively. First of all, the input data of the problem are stated. Afterward, the simulation results and discussions are presented.

The proposed controller is examined on a Danish test house with 4 rooms, including one kitchen, one bathroom, and two bedrooms with a height of 2.5 m. Fig. 12 sketches the schematic of the 150 $m^2$ Danish test house. Rooms 1, 2, and 4 have wooden flooring and Room 3 has a light concrete floor. The windows are double-layered with 80% transparency of the provided dimension in the figure. The materials of the walls and ceiling are lightweight concrete and gypsum with insulation [57].

The original sensor data is collected from 50 days' worth of data with 60 s resolution in March and April 2020. The 5 days' worth of data, equivalent to 7200 min, are used to train the CTSM. Fig. 13 presents the data for the 5 days including the heat consumption, solar power, waste heat from home appliances, and indoor air temperature.

Fig. 14 illustrates the sensor data of the ambient temperature with the deviation bounds. In this figure, the ambient temperatures are described by an expected (nominal value) and a set of positive/negative deviations. The lower and upper thresholds of ambient temperature are −4 °C and +4 °C, respectively. Fig. 15 presents the DHW consumption of

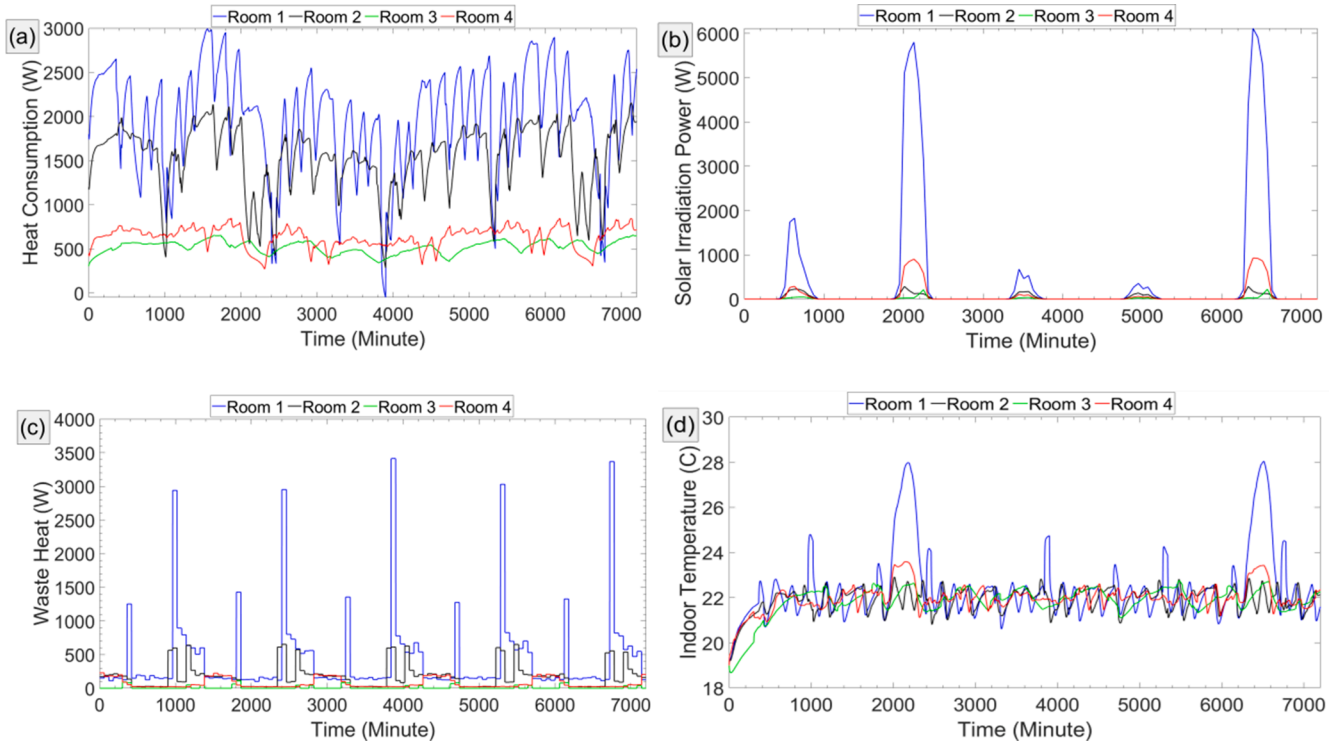


**Fig. 13.** The sensor data of the test house for the 5 days' training process (a) Heat consumption (b) Solar irradiation power (c) Waste heat of household appliances (d) Indoor temperature.

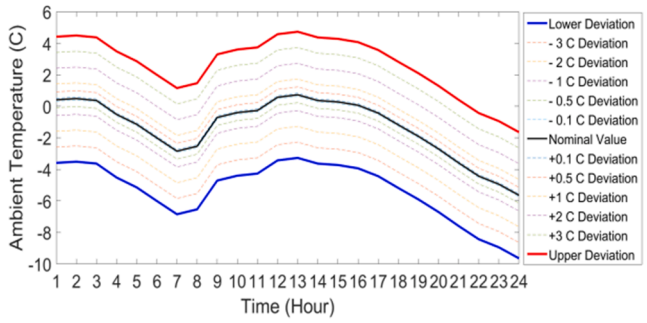


**Fig. 14.** Ambient temperature with positive (+4 °C) and negative (−4 °C) deviations.

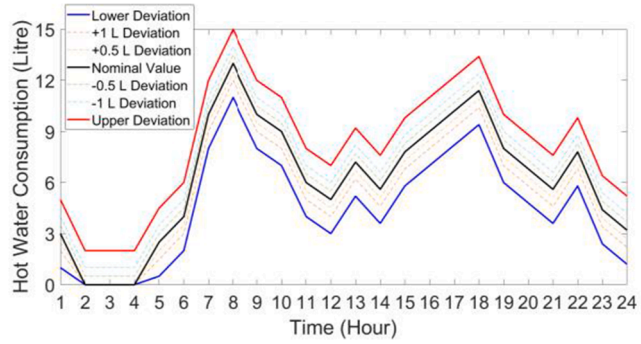


**Fig. 15.** DHW consumption with positive (+2 L/h) and negative deviation (−2 L/h).

the household with deviation bounds. The nominal DHW consumption is considered 150 Liter a day. Regarding the positive and negative deviations as ±2 L/h, the lower and upper daily consumptions are assumed 198 and 102 L/day.

In order to investigate the role of the uncertain variables on the operation of the heating system, three case studies are addressed.

In Case Study 1, the impacts of electricity price scenarios are evaluated. In this way, the expected values of weather data and DHW consumption are used. The electricity price scenarios are imported to stochastic programming.

In Case Study 2, the impacts of ambient temperature on the operation of the space heating system and CCWT are investigated. Different positive/negative deviations of the weather variables are imported to the problem to receive the response of the heating system.

In Case Study 3, the impacts of DHW consumption on the operation of water heating and OCWT are evaluated. In this way, the deviation bounds of DHW consumption are imported to the problem.

To present the simulation results, first of all, Fig. 16 describes the thermal dynamics of four rooms extracted by the CTSM. The CTSM is coded in language R. To identify the thermal model, 5 day's worth of sensor data, i.e. 7200 min, is used. The results state the coefficients of the thermal dynamics, Eqs. (1)–(3). Moreover, a graphical comparison between the predicted and actual temperatures is made. As can be seen, the CTSM predicts the air temperature of rooms 2, 3, and 4 reasonably well. In these cases, the residual temperatures, i.e. the difference between the predicted and actual values, are minor. Adversely, room 1 follows a different pattern. In this room, the residual temperatures are higher than the other rooms. The reason is that the household appliances, e.g. oven and refrigerator, generate heating power which is not captured by the thermal dynamic model. The waste heat from the kitchen appliances increases the residual temperatures in room 1.

Fig. 17 illustrates the power procurement strategies of the SEMPC in the three trading floors of the Danish Electricity Market. Besides, the generated scenarios and the expected electricity prices are depicted. Subfigure (a) shows the operation strategies in the day-ahead market. As can be seen, the day-ahead market faces two peak hours, including 9–11 and 18–20. The controller minimizes energy consumption in peak hours. In contrast, during off-peak hours 1–7 and 14–17, the controller increases the energy consumption. The controller schedules the main power consumption of the heating system based on energy price 24 h before energy delivery time. Subfigure (b) describes the energy trading in the intraday market. The intraday price is confronted with a substantial increase in hours 11 and 18–20. Therefore, the controller sells some parts of prepurchased energy to the intraday market. Adversely, the controller increases the power procurement from the intraday market when the electricity price is low, e.g. hours 1–4 and 21–22. Consequently, the controller adjusts the energy consumption based on the power availability 60–10 min before power delivery time. Subfigure (c) depicts the operation strategies in the balancing market. As the graph reveals, the balancing market faces a considerable increase in hours

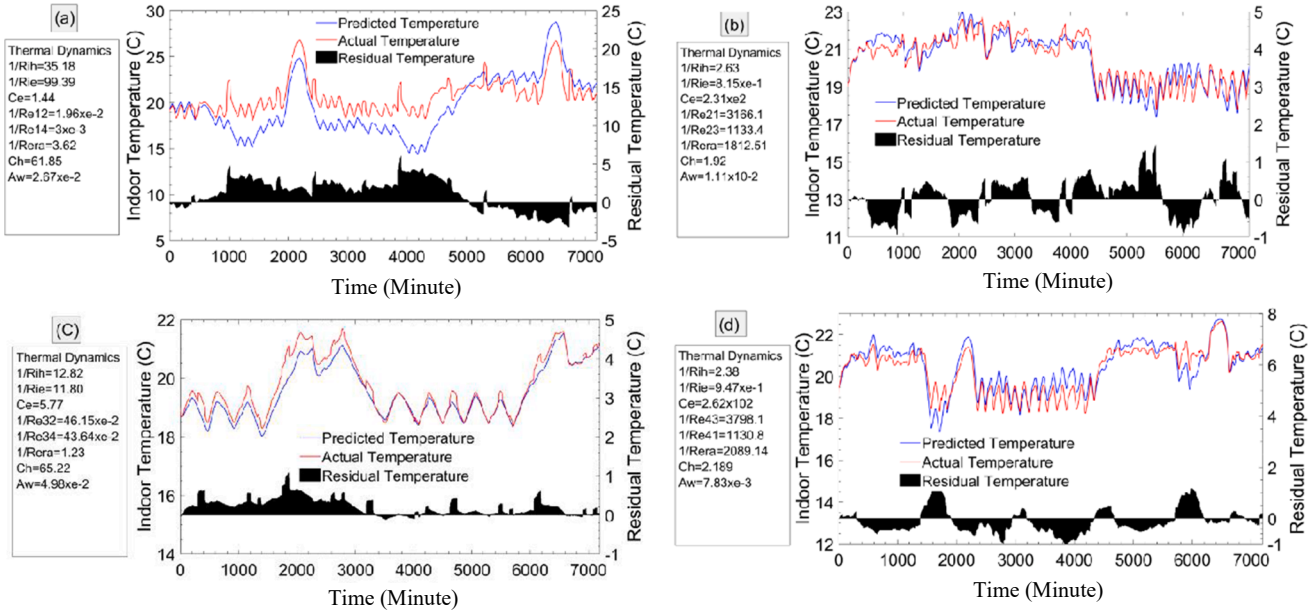


**Fig. 16.** Thermal dynamics of four rooms with a comparison between the predicted and measured temperatures (a) Room 1 (b) Room 2 (c) Room 3 (d) Room 4 [52].

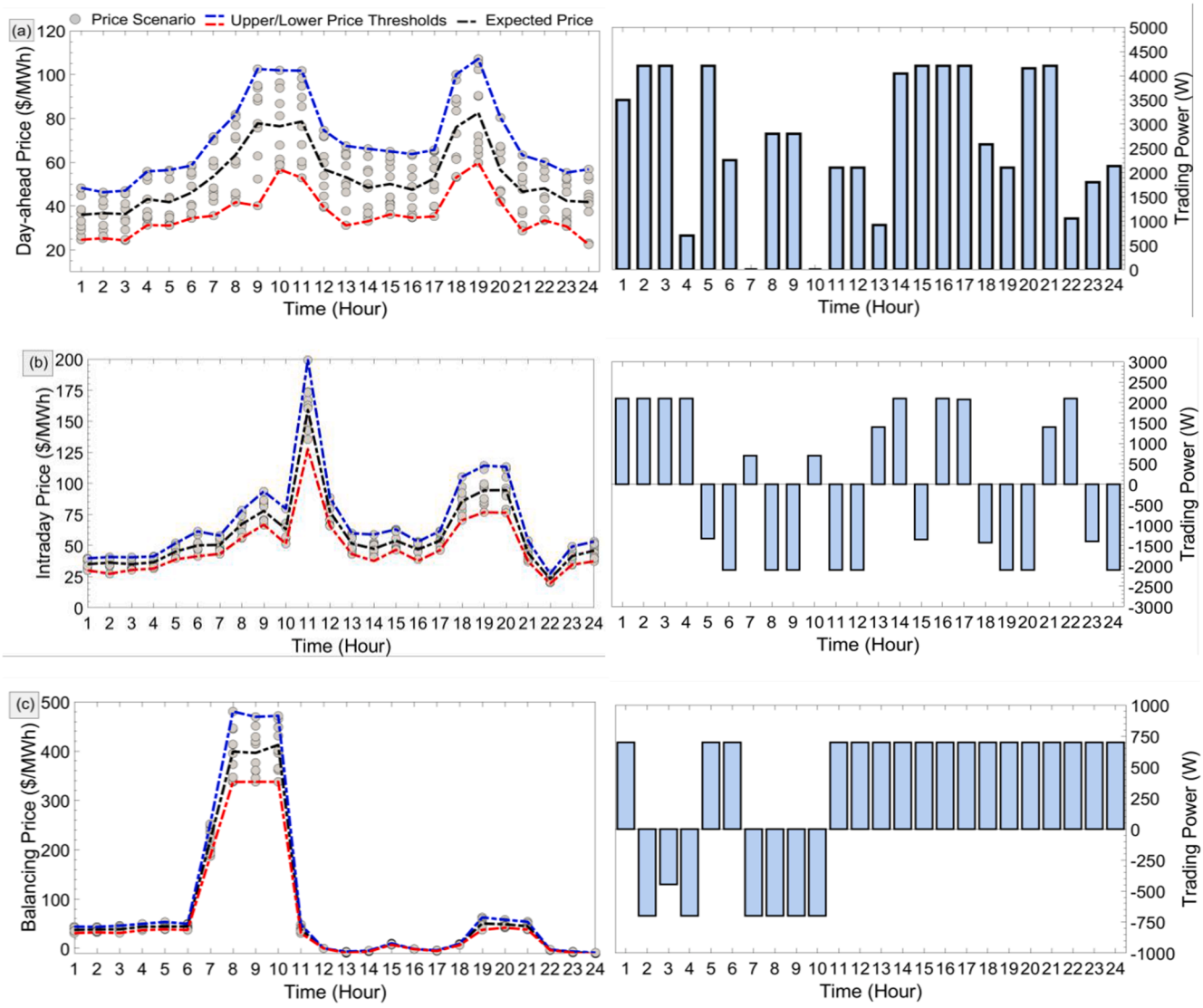


**Fig. 17.** Power procurement from the market floors for Case Study 1 (a) The day-ahead (b) The Intraday (c) The balancing.

8–10. The huge jump in the real-time price indicates a severe power shortage on the supply side. In response, the controller sells a part of prepurchased energy to the balancing market to make up-regulation for the supply network. In contrast, the market experiences low price hours during hours 12–24. In this duration, the balancing prices are zero or negative in some hours. Therefore, a power excess occurs on the supply side. The zero/negative prices motivate the controller to consume electricity. As a result, the controller increases the energy consumption to provide down-regulation for the power grid. Finally, subfigure (d) shows the net energy consumption of the heating system. In this subfigure, the expected electricity prices of the three market floors are also depicted. Based on the graph, the SEMPC minimizes the energy consumption during high price hours, i.e. power shortage, and maximizes the energy usage during high price hours, i.e. power shortage. The controller not only provides flexibility for the supply-side but also decreases the energy consumption cost of the household.

Regarding Case Study 2, Fig. 18 describes the operation of heating systems in response to the positive/negative deviations of the outdoor temperature. In this way, the indoor temperature and heating demand of the four rooms are presented. These figures are plotted for 12 deviation bounds in comparison with the nominal (expected) value. As the profiles of indoor temperature reveal, the heat controller satisfies the residents' comfort bounds for all rooms during ±4 °C deviations of ambient temperature. Making a comparison between the four rooms, the temperature profile of room 1 is considerably affected by the deviations of outdoor temperature. In contrast, the temperature of room 3 is less affected by the deviations of ambient temperature. The reason is that room 1 has the most building envelopes in common with the unconditioned environment. Besides, it has the largest window dimensions among the rooms. Adversely, room 3 has the lowest enclosures with the outdoor environment as well as the smallest window dimension. As a result, increasing the temperature deviation from the expected value, the variation of indoor temperature increases as the common envelope between conditioned and unconditioned environments increases. Moreover, the variation of indoor temperature during occupied hours, e.g. 1–6 and 17–24, is less than the unoccupied hours, e.g. 9–16. It shows that the EMPC adopts more robust heating strategies against the temperature deviations for occupied hours in comparison with the unoccupied hours.

Regarding the profiles of heating energy, the daily energy consumptions of rooms are shown by energy tags. Based on the heat demand of room 1, the lower and upper deviations in the outdoor temperature change the daily heating consumption from 35.04 kWh to 43.51 kWh (+24.17) and 27.77 kWh (−20.74%), respectively. For the upper and lower thresholds of temperature deviations, rooms 3 and 4 have experienced the highest reduction and increase in the heating consumption,

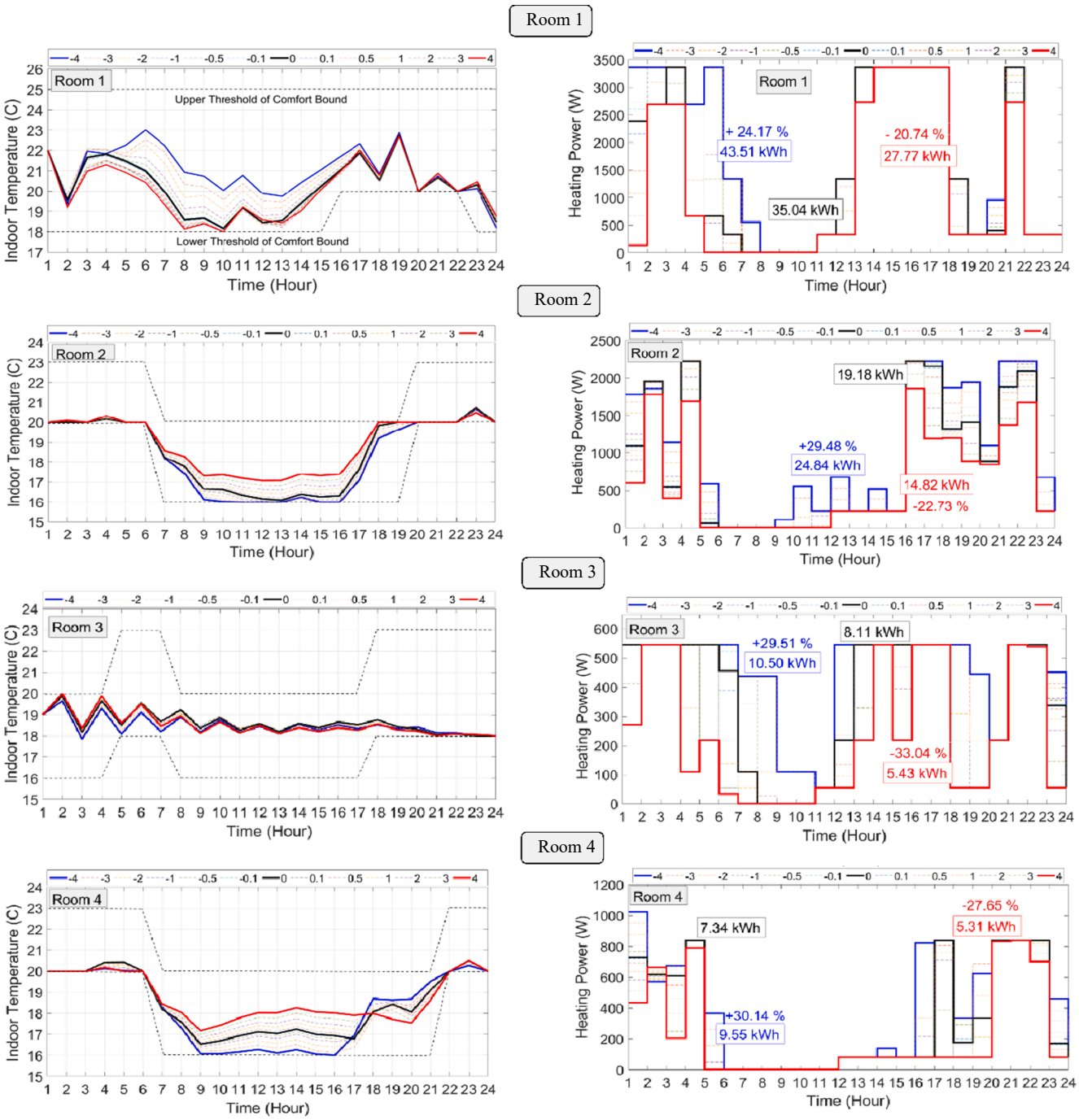


**Fig. 18.** Operation of heating systems of 4 rooms in response to deviation bounds of the outdoor temperature, Case Study 2.

around −33.04% and +30.14%, respectively.

Fig. 19 presents the water temperature of CCWT in response to different deviation bounds of ambient temperature. Moreover, the average water temperature is stated by the solid text boxes. Based on the graph, as the ambient temperature decreases, the water temperature decreases, especially during unoccupied hours 8–13. Besides, the ±4 deviations of ambient temperature change the average water temperature from 51.48 °C to 49.10 °C and 51.85 °C, for lower and upper thresholds, respectively. Most temperature changes occur in night hours 1–5 and unoccupied hours 8–13. Barely considerable change is seen in the other occupied hours. For all the deviations, the controller maintains the water temperature within the upper/lower thresholds of water temperature.

Fig. 20 describes the operational strategies of the OCWT, including the water temperature and heat consumption, in response to the deviation bounds of the DHW consumption as Case Study 3. The daily nominal value of DHW consumption is considered 150 L for a family of four. In the lower and upper deviation bounds, the DHW consumption deviates ±2 L/h (±48 L/day). Therefore, the lower and upper thresholds of the daily DHW consumption are confined to 102 and 198 L. In this way, subfigure (a) illustrates the temperature of hot water. Based on the graph, the heat controller maintains the water temperature within the comfort bound $45 \leq \theta_w^{CC} \leq 60$ for all the deviation bounds. The solid boxes describe the average DHW temperature. The average temperatures experience minor changes in comparison to the expected value of DHW consumption. Subfigure (b) presents the heating consumption of the OCWT. As can be seen, the lower deviation of the DHW consumption

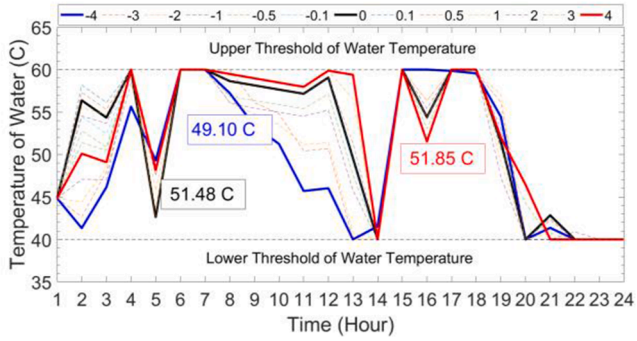


**Fig. 19.** The water temperature of CCWT in response to ambient temperature, Case Study 2.

decreases the energy consumption of the OCWT from 24.22 kWh to 17.95 kWh. In contrast, the upper deviation increases the heating consumption to 31.22 kWh. As a result, the controller changes the heating consumption by +28.90% and −25.88% to maintain the same level for the DHW temperature against the deviations of DHW consumption.

Fig. 21 shows the economic analysis of the heating system for three case studies. The bar graphs indicate the power consumption cost of the heating system in the three electricity markets. Moreover, the operations costs are presented for three states, including the base case, high/low thresholds of the associated uncertain variable. Regarding Case Study 1, considerable changes are seen from the based case to the upper/lower price thresholds. In this way, pernicious and propitious facets of electricity price uncertainty increase the total cost from 49.50 to 72.17 and 24.76, respectively. In Case Study 2, the operation cost of the heating system is less affected in comparison to Case Study 1. The results show that the upper and lower thresholds of ambient temperature change the energy consumption cost from 49.50 to 27.13 and 76.98, respectively. The lowest change in the operation cost is seen in Case Study 3. The upper and lower thresholds of the DHW consumption change the operation cost from 49.50 to 52.74 and 46.52. The uncertainties of electricity price and DHW consumption have the highest and lowest impacts on the operation costs of the residential heating system, respectively.

It is worthy to make a comparison between the proposed controller and some recent studies. The fundamentals of the thermal dynamic are extracted from [53]. This study proposed the CTSM and surveyed different RC networks for residential buildings. The test house of the

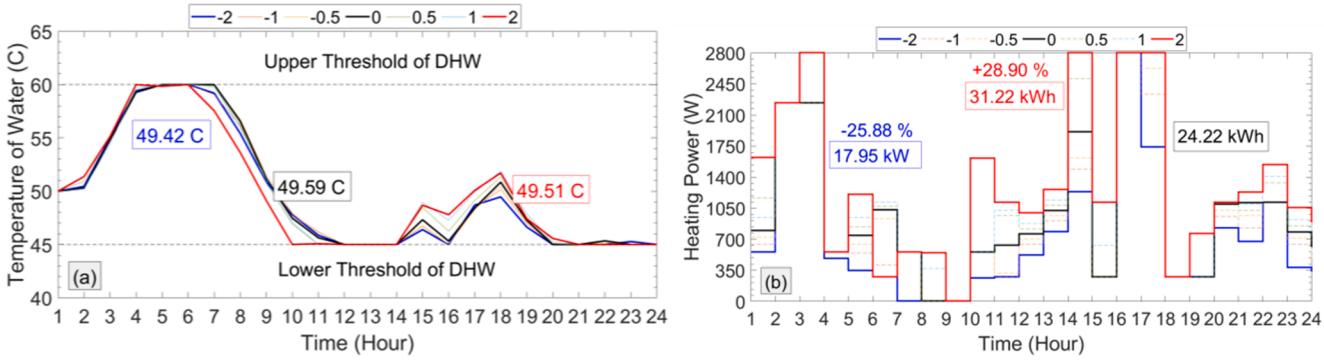


**Fig. 20.** Operational strategies of OCWT in response to deviations of DHW consumption, Case Study 3 (a) Temperature of DHW (b) Heating consumption.

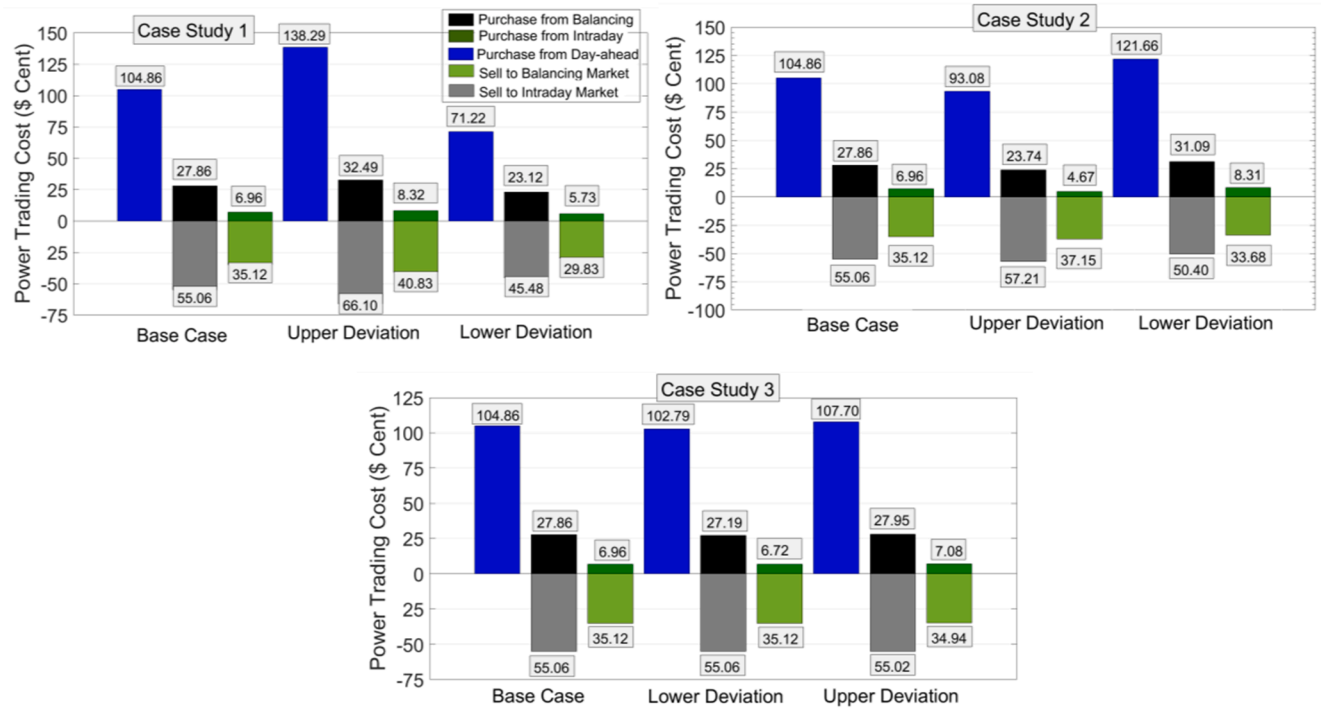


**Fig. 21.** Economic analysis of three case studies in the electricity market floors.

current study is examined in [51] to provide day-ahead peak-shaving for the Danish electricity market. The suggested controller in the research study [52] addressed intraday and balancing markets to adjust power imbalances from 60 min ahead until near real-time. In current study, two main contributions are made as (1) optimizing the DHW of the households (2) examining the operation of the heating system for different deviations of the weather variables and DHW consumption. In [58], heat control is designed for space heating and DHW to flatten the peak profile of the residential sector. The controller provided up to 35% peak reduction when both the space heating and DHW contribute to the power flexibility. In contrast, the research study [59] unlocked the flexibility opportunities of residential heat pumps in the frequency restoration reserve market.

To survey the main features of the suggested controller, the advantages and challenges are stated. First of all, the key positive points can be stated as follows:

1. The controller responds effectively to dynamic electricity prices in the three market floors. Assuming a correlation between electricity price and RES availability, the controller can unlock the power flexibility of the residential heating system when a renewable power shortage/excess occurs.
2. Considering the water storage tanks, the predictive controller reduces the power consumption in high price hours while satisfying the residents' comfort. The controller heats the water tanks in low price hours to supply the space heating and DHW in high price hours.
3. The economic objective function of the controller reduces the energy bill of the households. The residential heating system is supplied with low energy prices during low electricity prices when the power system faces renewable energy excess.

Although the controller takes the abovementioned advantages, the following challenges may be subject to the further investigation:

1. The small-scale consumers, e.g. a single-family house, do not take part in the wholesale electricity markets. To overcome this barrier, the district heating aggregators should be addressed to integrate the heat-power flexibility of a significant number of households into the supply side.
2. Despite the district heating system, the heat pumps may be shared with some buildings instead of a single house. The optimization of shared heat pumps for buildings with different thermal dynamics may be subject to new studies. Besides, the sewage water can be addressed as the thermal source instead of the air-source heat pump.
3. In this approach, complete input data is used to train the controller. In district heating studies, barely such detailed data are available to optimize the operation of the district heating. Moreover, modeling the complex differential equations for a significant number of buildings, the complexity of the problem increases considerably and the problem may be intractable. Therefore, the mathematical model may be relaxed to simple linear equations not only to make the problem tractable but also to estimate the thermal dynamics with data scarcity.

## 5. Conclusion

This paper proposed a heat controller for residential heat pumps to supply the space heating and domestic hot water consumption in presence of uncertain variables, including electricity prices, ambient temperature, and hot water consumption. To extract the thermal dynamics of the building, Continuous-Time Stochastic Model was addressed using 5 days' worth of sensor data. Stochastic economic model predictive control was suggested to incorporate the electricity price uncertainties into the three stages of daily electricity markets, i.e. the day-ahead, intraday, and balancing markets. The imperfect data of ambient temperature and domestic hot water consumption were modeled by envelope bounds with positive and negative deviations. Consequently, the operational strategies of the heat controller were evaluated in response to the uncertain variables. To sum up, the following key points were pointed out:

1. The developed thermal dynamics of the Continuous-Time Stochastic Model made it possible to address multiple temperature zones. The accuracy of the suggested approach was reasonably high for rooms without sensible waste heat. For the kitchen with waste heat from ovens and refrigerators, the accuracy is relatively lower than the other rooms.
2. The heat controller unlocked flexibility opportunities of the residential heating system in response to market price scenarios hierarchically. In this way, the controller (1) provided power flexibility for the day-ahead market on long notice, 24 h prior to energy delivery time (2) adjusted power flexibility in the intraday market on mid notice, one hour before energy delivery time, and (3) finally, provided up-/down-regulation for the balancing market on short notice, a few seconds before energy delivery time.
3. The predictive controller heated up the water tanks, for both space heating and domestic hot water, in low price hours to regulate power consumption at the opposite side of the power system imbalance. The stored energy in the water tanks supplied the radiators and hot water consumptions during high price hours.
4. The economic analysis showed that the uncertainties associated with electricity price and ambient temperature have more impacts on the household energy cost than the uncertainty of domestic hot water consumption.
5. In practical electricity markets, the residential heating systems participate in the electricity market through intermediary agents, e.g. district heating aggregators. The aggregators integrate the flexibility potentials of a significant number of households into the electricity market.
6. To design heat controllers in district heating, mathematical relaxation may be required to (1) extract the thermal dynamics of the buildings with data scarcity (2) make the problem tractable when a significant number of residential buildings are aggregated.

## CRediT authorship contribution statement

**Hessam Golmohamadi:** Conceptualization, Methodology, Software, Data curation, Writing – original draft.

## Declaration of Competing Interest

The authors declare that they have no known competing financial interests or personal relationships that could have appeared to influence the work reported in this paper.

## References

[1] "International Energy Agency, IEA; 2020.
[2] Golmohamadi H, Keypour R, Bak-Jensen B, Pillai JR. A multi-agent based optimization of residential and industrial demand response aggregators. Int J Electr Power Energy Syst 2019;107:472–85. https://doi.org/10.1016/j.ijepes.2018.12.020.
[3] Golmohamadi H, Asadi A. A multi-stage stochastic energy management of responsive irrigation pumps in dynamic electricity markets. Appl Energy 2020;265:114804. https://doi.org/10.1016/j.apenergy.2020.114804.
[4] Golmohamadi H, Asadi A. Integration of joint power-heat flexibility of oil refinery industries to uncertain energy markets. Energies 2020;13(18). https://doi.org/10.3390/en13184874.
[5] Daryabari MK, Keypour R, Golmohamadi H. Stochastic energy management of responsive plug-in electric vehicles characterizing parking lot aggregators. Appl Energy 2020;279:115751. https://doi.org/10.1016/j.apenergy.2020.115751.
[6] Golmohamadi H, Keypour R, Bak-Jensen B, Radhakrishna Pillai J. Optimization of household energy consumption towards day-ahead retail electricity price in home energy management systems. Sustain Cities Soc 2019;47:101468. https://doi.org/10.1016/j.scs.2019.101468.

[7] Golmohamadi H. Agricultural demand response aggregators in electricity markets: structure, challenges and practical solutions- a tutorial for energy experts. Technol Econ Smart Grids Sustain Energy 2020;5(1):17. https://doi.org/10.1007/s40866-020-00091-7.

[8] Golmohamadi H, Keypour R, Bak-Jensen B, Pillai JR, Khooban MH. Robust self-scheduling of operational processes for industrial demand response aggregators. IEEE Trans Ind Electron 2020;67(2):1387–95. https://doi.org/10.1109/TIE.2019.2899562.

[9] Daryabari MK, Keypour R, Golmohamadi H. Robust self-scheduling of parking lot microgrids leveraging responsive electric vehicles. Appl Energy 2021;290:116802. https://doi.org/10.1016/j.apenergy.2021.116802.

[10] Tschopp D, Tian Z, Berberich M, Fan J, Perers B, Furbo S. Large-scale solar thermal systems in leading countries: a review and comparative study of Denmark, China, Germany and Austria. Appl Energy 2020;270:114997. https://doi.org/10.1016/j.apenergy.2020.114997.

[11] Huang Y, Zhang Y, Xie Y, Zhang Y, Gao X, Ma J. Long-term thermal performance analysis of deep coaxial borehole heat exchanger based on field test. J Clean Prod 2021;278:123396. https://doi.org/10.1016/j.jclepro.2020.123396.

[12] Merkel E, McKenna R, Fehrenbach D, Fichtner W. A model-based assessment of climate and energy targets for the German residential heat system. J Clean Prod 2017;142:3151–73. https://doi.org/10.1016/j.jclepro.2016.10.153.

[13] Wang D, et al. Optimal scheduling strategy of district integrated heat and power system with wind power and multiple energy stations considering thermal inertia of buildings under different heating regulation modes. Appl Energy 2019;240:341–58. https://doi.org/10.1016/j.apenergy.2019.01.199.

[14] Finck C, Li R, Kramer R, Zeiler W. Quantifying demand flexibility of power-to-heat and thermal energy storage in the control of building heating systems. Appl Energy 2018;209:409–25. https://doi.org/10.1016/j.apenergy.2017.11.036.

[15] Vivian J, Quaggiotto D, Zarrella A. Increasing the energy flexibility of existing district heating networks through flow rate variations. Appl Energy 2020;275:115411. https://doi.org/10.1016/j.apenergy.2020.115411.

[16] Le Dréau J, Heiselberg P. Energy flexibility of residential buildings using short term heat storage in the thermal mass. Energy 2016;111:991–1002. https://doi.org/10.1016/j.energy.2016.05.076.

[17] Foteinaki K, Li R, Péan T, Rode C, Salom J. Evaluation of energy flexibility of low-energy residential buildings connected to district heating. Energy Build 2020;213:109804. https://doi.org/10.1016/j.enbuild.2020.109804.

[18] Meesenburg W, Ommen T, Thorsen JE, Elmegaard B. Economic feasibility of ultra-low temperature district heating systems in newly built areas supplied by renewable energy. Energy 2020;191:116496. https://doi.org/10.1016/j.energy.2019.116496.

[19] Brandi S, Piscitelli MS, Martellacci M, Capozzoli A. Deep reinforcement learning to optimise indoor temperature control and heating energy consumption in buildings. Energy Build 2020;224:110225. https://doi.org/10.1016/j.enbuild.2020.110225.

[20] Moallemi A, Arabkoohsar A, Pujatti FJP, Valle RM, Ismail KAR. Non-uniform temperature district heating system with decentralized heat storage units, a reliable solution for heat supply. Energy 2019;167:80–91. https://doi.org/10.1016/j.energy.2018.10.188.

[21] Saloux E, Candanedo JA. Modelling stratified thermal energy storage tanks using an advanced flowrate distribution of the received flow. Appl Energy 2019;241:34–45. https://doi.org/10.1016/j.apenergy.2019.02.075.

[22] Yan T, Wang RZ, Li TX, Wang LW, Fred IT. A review of promising candidate reactions for chemical heat storage. Renew Sustain Energy Rev 2015;43:13–31. https://doi.org/10.1016/j.rser.2014.11.015.

[23] De Schepper G, Paulus C, Bolly P-Y, Hermans T, Lesparre N, Robert T. Assessment of short-term aquifer thermal energy storage for demand-side management perspectives: experimental and numerical developments. Appl Energy 2019;242:534–46. https://doi.org/10.1016/j.apenergy.2019.03.103.

[24] Naranjo-Mendoza C, Oyinlola MA, Wright AJ, Greenough RM. Experimental study of a domestic solar-assisted ground source heat pump with seasonal underground thermal energy storage through shallow boreholes. Appl Therm Eng 2019;162:114218. https://doi.org/10.1016/j.applthermaleng.2019.114218.

[25] Nie B, Palacios A, Zou B, Liu J, Zhang T, Li Y. Review on phase change materials for cold thermal energy storage applications. Renew Sustain Energy Rev 2020;134:110340. https://doi.org/10.1016/j.rser.2020.110340.

[26] Zhang S, Wang Z. Thermodynamics behavior of phase change latent heat materials in micro-/nanoconfined spaces for thermal storage and applications. Renew Sustain Energy Rev 2018;82:2319–31. https://doi.org/10.1016/j.rser.2017.08.080.

[27] Blanco I, Andersen AN, Guericke D, Madsen H. A novel bidding method for combined heat and power units in district heating systems. Energy Syst 2019. https://doi.org/10.1007/s12667-019-00352-0.

[28] Blanco I, Guericke D, Andersen AN, Madsen H. Operational planning and bidding for district heating systems with uncertain renewable energy production. Energies 2018;11(12). https://doi.org/10.3390/en11123310.

[29] Powell KM, et al. Thermal energy storage to minimize cost and improve efficiency of a polygeneration district energy system in a real-time electricity market. Energy 2016;113:52–63. https://doi.org/10.1016/j.energy.2016.07.009.

[30] Dahash A, Ochs F, Janetti MB, Streicher W. Advances in seasonal thermal energy storage for solar district heating applications: a critical review on large-scale hot-water tank and pit thermal energy storage systems. Appl Energy 2019;239:296–315. https://doi.org/10.1016/j.apenergy.2019.01.189.

[31] Hennessy J, Li H, Wallin F, Thorin E. Flexibility in thermal grids: a review of short-term storage in district heating distribution networks. Energy Procedia 2019;158:2430–4. https://doi.org/10.1016/j.egypro.2019.01.302.

[32] Salpakari J, Mikkola J, Lund PD. Improved flexibility with large-scale variable renewable power in cities through optimal demand side management and power-to-heat conversion. Energy Convers Manag 2016;126:649–61. https://doi.org/10.1016/j.enconman.2016.08.041.

[33] Vandermeulen A, van der Heijde B, Helsen L. Controlling district heating and cooling networks to unlock flexibility: a review. Energy 2018;151:103–15. https://doi.org/10.1016/j.energy.2018.03.034.

[34] Dominković DF, Junker RG, Lindberg KB, Madsen H. Implementing flexibility into energy planning models: soft-linking of a high-level energy planning model and a short-term operational model. Appl Energy 2020;260:114292. https://doi.org/10.1016/j.apenergy.2019.114292.

[35] Balić D, Maljković D, Lončar D. Multi-criteria analysis of district heating system operation strategy. Energy Convers Manag 2017;144:414–28. https://doi.org/10.1016/j.enconman.2017.04.072.

[36] Peeters L, Van der Veken J, Hens H, Helsen L, D'haeseleer W. Control of heating systems in residential buildings: current practice. Energy Build 2008;40(8):1446–55. https://doi.org/10.1016/j.enbuild.2008.02.016.

[37] Kitapbayev Y, Moriarty J, Mancarella P. Stochastic control and real options valuation of thermal storage-enabled demand response from flexible district energy systems. Appl Energy 2015;137:823–31. https://doi.org/10.1016/j.apenergy.2014.07.019.

[38] Zhang Y, Xia J, Fang H, Jiang Y, Liang Z. Field tests on the operational energy consumption of Chinese district heating systems and evaluation of typical associated problems. Energy Build 2020:110269. https://doi.org/10.1016/j.enbuild.2020.110269.

[39] Yang X, Svendsen S. Improving the district heating operation by innovative layout and control strategy of the hot water storage tank. Energy Build 2020. https://doi.org/10.1016/j.enbuild.2020.110273.

[40] Neirotti F, Noussan M, Riverso S, Manganini G. Analysis of different strategies for lowering the operation temperature in existing district heating networks. Energies 2019;12(2). https://doi.org/10.3390/en12020321.

[41] Bak Y, Lee K-B. Development of PCS to utilize differential pressure energy in district heating systems with reduced DC-link voltage variation. J Power Electron 2020;20(4):1109–18. https://doi.org/10.1007/s43236-020-00091-x.

[42] Arabzadeh V, Alimohammadisagvand B, Jokisalo J, Siren K. A novel cost-optimizing demand response control for a heat pump heated residential building. Build Simul 2018;11(3):533–47. https://doi.org/10.1007/s12273-017-0425-5.

[43] Laajalehto T, Kuosa M, Mäkilä T, Lampinen M, Lahdelma R. Energy efficiency improvements utilising mass flow control and a ring topology in a district heating network. Appl Therm Eng 2014;69(1):86–95. https://doi.org/10.1016/j.applthermaleng.2014.04.041.

[44] Patteeuw D, Helsen L. Combined design and control optimization of residential heating systems in a smart-grid context. Energy Build 2016;133:640–57. https://doi.org/10.1016/j.enbuild.2016.09.030.

[45] Hietaharju P, Ruusunen M, Leiviskä K. Enabling demand side management: heat demand forecasting at city level. Materials (Basel) 2019;12(2). https://doi.org/10.3390/ma12020202.

[46] Tang R, Wang S. Model predictive control for thermal energy storage and thermal comfort optimization of building demand response in smart grids. Appl Energy 2019;242:873–82. https://doi.org/10.1016/j.apenergy.2019.03.038.

[47] Kuboth S, Heberle F, König-Haagen A, Brüggemann D. Economic model predictive control of combined thermal and electric residential building energy systems. Appl Energy 2019;240:372–85. https://doi.org/10.1016/j.apenergy.2019.01.097.

[48] Wernstedt Fredrik. Multi-agent systems for distributed control of district heating systems. Blekinge Institute of Technology; 2005.

[49] Agesen MK, et al. Toolchain for user-centered intelligent floor heating control. In: IECON 2016 - 42nd Annual Conference of the IEEE Industrial Electronics Society; 2016. p. 5296–301. doi: 10.1109/IECON.2016.7794040.

[50] Dengiz T, Jochem P, Fichtner W. Demand response with heuristic control strategies for modulating heat pumps. Appl Energy 2019;238:1346–60. https://doi.org/10.1016/j.apenergy.2018.12.008.

[51] Golmohamadi H, Guldstrand Larsen K, Gjøl Jensen P, Riaz Hasrat I. Optimization of power-to-heat flexibility for residential buildings in response to day-ahead electricity price. Energy Build 2021;232:110665. https://doi.org/10.1016/j.enbuild.2020.110665.

[52] Golmohamadi H, Larsen KG, Jensen PG, Hasrat IR. Hierarchical flexibility potentials of residential buildings with responsive heat pumps: a case study of Denmark. J Build Eng 2021;41:102425. https://doi.org/10.1016/j.jobe.2021.102425.

[53] Bacher P, Madsen H. Identifying suitable models for the heat dynamics of buildings. Energy Build 2011;43(7):1511–22. https://doi.org/10.1016/j.enbuild.2011.02.005.

[54] Juhl R, Kristensen NR, Bacher P, Kloppenborg J, Madsen H. Grey-box modeling of the heat dynamics of a building with CTSM-R; 2020. [Online]. Available: http://ctsm.info/building2.pdf.

[55] D. DTU Compute, "Continuous Time Stochastic Modelling for R (CTSM); 2021. http://ctsm.info/index.html.

[56] Xu Z, Diao R, Lu S, Lian J, Zhang Y. Modeling of electric water heaters for demand response: a baseline PDE model. IEEE Trans Smart Grid 2014;5(5):2203–10. https://doi.org/10.1109/TSG.2014.2317149.

[57] Vinther K, Green T, Jensen SØ, Bendtsen JD. Predictive Control of Hydronic Floor Heating Systems using Neural Networks and Genetic Algorithms**This work was financially supported by the Danish Energy Agency through the EUDP project OpSys (jn:64014–0548) and the Faculty of Engineering and Science at Aalborg

University. IFAC-PapersOnLine 2017;50(1):7381–8. https://doi.org/10.1016/j.ifacol.2017.08.1477.

[58] Vivian J, Prataviera E, Cunsolo F, Pau M. Demand Side Management of a pool of air source heat pumps for space heating and domestic hot water production in a residential district. Energy Convers Manag 2020;225:113457. https://doi.org/10.1016/j.enconman.2020.113457.

[59] Romero Rodríguez L, Brennenstuhl M, Yadack M, Boch P, Eicker U. Heuristic optimization of clusters of heat pumps: a simulation and case study of residential frequency reserve. Appl Energy 2019;233–234:943–58. https://doi.org/10.1016/j.apenergy.2018.09.103.